*Electronic Research Archive*

https://www.aimspress.com/journal/era

ERA, 33(11): 6885–6921.
DOI: 10.3934/era.2025304
Received: 30 September 2025
Revised: 30 October 2025
Accepted: 05 November 2025
Published: 17 November 2025

*Research article*

# Artificial viscosity penalty-projection finite element approximations of non-Newtonian fluid flow for aneurysmal disease

**Keqing Feng**[1], **Yingchun Shan**[2] **and Guang-an Zou**[1,*]

[1] School of Mathematics and Statistics, Henan University, Kaifeng 475000, China
[2] College of Mathematics and System Sciences, Xinjiang University, Urumqi 830046, China

* **Correspondence:** Email: zouguangan@henu.edu.cn.

**Abstract:** In this paper, we propose a new formulation of the artificial-viscosity penalty finite element methods for solving the mathematical model of non-Newtonian blood flow, treating blood as a pseudo-plastic fluid obeying the power-law Navier-Stokes equations. The proposed schemes are based on the artificial-viscosity mixed finite element method in the spatial direction, combined with a backward-Euler scheme and penalty-projection scheme for temporal discretization. It is rigorously derived the stability and error estimates for the fully discrete schemes. Numerical examples are presented to validate the theoretical ideas and to demonstrate the effectiveness of our proposed strategies. The comparison shows that the artificial viscosity penalty-projection scheme demands less central processing unit time, as well as a slightly higher-order precision. Finally, the penalty-projection finite element scheme is successfully applied to study the influence of blood viscosity on hemodynamics in aortic aneurysms. Moreover, numerical investigations for flow patterns based on patient-specific geometric models of cerebral aneurysms through segmentation of magnetic resonance imaging have been performed. The present study clearly illustrates the importance of taking the non-Newtonian properties of blood flow within aneurysms into account when studying the risk of aneurysm rupture.

**Keywords:** power-law Navier-Stokes equations; artificial viscosity method; penalty-projection scheme; finite element method; aneurysmal disease

## 1. Introduction

Aneurysmal disease involes vessel enlargement and, in some cases, rupture, such as a cerebral aneurysm, which is an abnormal vascular dilation with a high risk of rupture. Aneurysmal ruptures can cause life-threatening intracranial hemorrhages and even death. It is very hard to find the aneurysms before they rupture because either there are no symptoms or the symptoms are non-specific and can be linked to other, more common conditions. Therefore, mathematical models incorporating

experimental observations can help us better understand the blood hemodynamics, arterial geometry and biomechanics, and the vessel environment in the onset, evolution, and rupture of aneurysms. Moreover, the computational fluid dynamic (CFD) model of blood flow plays an important role in the pathogenesis and treatment of aneurysmal disease. In this way, a great deal of research work has been done on arteries, treating blood as an incompressible Newtonian fluid; see [1–5] and the references cited therein. Likewise, many existing modeling studies of aneurysmal disease are based on the Newtonian fluid assumption [6–9]. The primary rationale for assuming Newtonian behavior is that the shear rates in large arteries are sufficiently high, a condition under which blood viscosity becomes approximately constant [10]. However, human blood is highly complex, as its viscosity depends on the shear rate. Blood viscosity is shear-thinning because of the disaggregation of the rouleaux (stacks of red blood cells) and the orientation of individual red blood cells. Experimental evidence has also shown that blood, under certain conditions, behaves as a nonlinear viscoelastic fluid, resulting from the elastic membranes of its constituents [11]. However, in steady-state flow conditions, especially when the flow reverses direction or stops, there are periods of time and spatial regions where low shear rates are encountered. Moreover, the blood flow may be affected by non-Newtonian behavior in pathologically altered configurations such as aneurysms and stenoses, where red blood cells and platelets can aggregate and thus change the bloods viscosity. Consequently, it is reasonable to infer that the non-Newtonian flow behavior could become important and thus cannot be neglected.

Indeed, many of the computational studies found in the literature on blood rheology gives a strong indication that, the non-Newtonian effects of blood flow cannot be neglected in a variety of geometries (see [12–16]). Even though some researchers have already investigated the effect of blood viscosity on the flow field inside the aneurysm by using different non-Newtonian models (for examples, see [16–21] and the references therein), most of the existing studies use highly simplified geometries (a simple curved tube or bifurcation), laminar flow only, steady-state flow only, or simplified turbulence models. Furthermore, the mathematical foundation and numerical analysis of the proposed methods have not been exhibited in these works. Nevertheless, the numerical algorithm and the corresponding theoretical analysis of the resulting problem is particularly important. Hence, the main emphasis of the present work is to highlight the numerical analysis of the proposed methods and to study the influence of blood viscosity on the hemodynamics in aneurysms. Moreover, numerical studies of flow patterns based on patient-specific geometric models of cerebral aneurysms through segmentation of medical images have been performed, which could help vascular surgeons in selecting the best surgical procedure for a patient.

Recent advances in non-Newtonian hemodynamic simulations have significantly improved our understanding of complex cardiovascular flows through innovative numerical approaches. Katz et al. [22] pioneered the integration of non-Newtonian models with high-resolution turbulence simulations, enabling accurate predictions of wall shear stress distributions in aortic coarctations and offering critical insights into the mechanisms of post-surgical restenosis. Complementing this work, [23] introduced physics-informed neural networks (PINNs) for real-time four-dimensional (4D) hemodynamic modeling. By embedding non-Newtonian constitutive relations into deep learning frameworks, their approach dramatically enhances computational efficiency, making it more suitable for clinical applications. Meanwhile, [24] developed a multiscale finite element method (FEM)-based model that integrates fluid-structure interaction (FSI) and microcirculation effects, allowing precise simulation of atherosclerotic blood flow dynamics under physiological conditions. Collectively, these studies represent a paradigm shift in hemodynamic modeling, transitioning from traditional CFD methods

to data-driven and multiphysics approaches and bridging the gap between theoretical research and clinical practice.

Although the power-law model is widely used to describe blood's shear-thinning behavior in aneurysmal flows, it introduces three key numerical and physical challenges that our work addresses by overcoming the limitations of existing methods. First, the power-law term exhibits severe nonlinearity at low shear rates, where the viscosity component becomes highly sensitive to small velocity gradients, often leading to numerical oscillations or divergence in a standard mixed FEM. Second, the tight coupling between the incompressibility constraint and power-law viscosity results in an ill-conditioned system for time-dependent pulsatile flows when traditional projection schemes are employed. Third, the power-law model's reduced solution regularity limits the accuracy of low-order FEMs or simplified turbulence models in capturing sharp shear gradients at aneurysm necks. Existing approaches often rely on simplified geometries [16] or omit convergence analyses [19], highlighting the need for a method that balances stability, accuracy, and patient-specific applicability. These challenges motivate our artificial viscosity penalty-projection finite element scheme, which mitigates oscillations, enforces incompressibility, and ensures rigorous stability and error bounds.

In the present study, the generalized power-law model has been adopted to investigate the shear-thinning behavior of blood flow in the diseased vessels. We consider the finite element approximation of non-Newtonian blood flows governed by the following incompressible power-law Navier-Stokes equations:

$$\begin{cases} \rho[\boldsymbol{u}_t + (\boldsymbol{u}\cdot\nabla)\boldsymbol{u}] - \nabla\cdot(\nu_0|\nabla\boldsymbol{u}|^{r-2}\nabla\boldsymbol{u}) + \nabla p = \boldsymbol{f},\ x\in\Omega, t>0, \\ \nabla\cdot\boldsymbol{u} = 0,\ x\in\Omega, t>0, \\ \boldsymbol{u}(\boldsymbol{x},0) = \boldsymbol{u}_0,\ x\in\Omega, \end{cases} \tag{1.1}$$

where $\Omega$ is the flow region, a bounded domain in $\mathbb{R}^d$ with $d = 2$ or 3, and $\partial\Omega$ its regular boundary. $\rho > 0$ is the density of blood and $\boldsymbol{u} = (\boldsymbol{u}_1(x), \cdots, \boldsymbol{u}_d(x))$ is the velocity of a fluid particle located at $x = (x_1, \cdots, x_d)$; $\nabla\cdot\boldsymbol{u} = \Sigma_i^d \partial\boldsymbol{u}_i/\partial x_i$ is the divergence of $\boldsymbol{u}$; $\nabla p$ is the gradient of the blood pressure; and $\boldsymbol{f}$ represents the external body forces. The parameter $\nu_0 > 0$ is a constant and we assume $1 < r \le 2$, which is obeys the power law for a pseudo-plastic. Noting that the choice $r = 2$ in (1.1) leads to the Laplacian operator, the system is just the classical Navier-Stokes equations.

Up to the present, many researchers have proposed the mixed FEM for studying the steady-state power-law Stokes flow, which lack the terms of time-derivatives and convective in (1.1), such as the works of Barrett and Liu [25, 26], Baranger et al. [27], and Lefton and Wei [28], just to mention a few. However, it should be mentioned that no numerical experiments are exhibited in these works. In addition, a penalty finite element approximation of the stationary power-law Stokes problem was established in a series of papers [29–31]. It should be noted that the governing equations in (1.1) are highly nonlinear because of the nonlinear function of the shear rate and he convective term. Due to the presence of severe nonlinearity combined with the pressure and the incompressibility condition, it is clear that finding the analytical solution of (1.1) is extremely complicated. As far as is known, there is very little research devoted to he numerical analysis of (1.1) in the literature; moreover, these are the first results based on the artificial viscosity penalty finite element framework dealing with the non-stationary power-law Navier-Stokes equations. The main ideas of this algorithm are given below. We analyze, mathematically and numerically, an artificial viscosity penalty method for (1.1) to approximate the

solution $(\boldsymbol{u}, p)$ with $(\boldsymbol{u}^\varepsilon, p^\varepsilon)$, which corresponds to the following penalty system:

$$\begin{cases} \rho[\boldsymbol{u}_t^\varepsilon + \widetilde{B}(\boldsymbol{u}^\varepsilon, \boldsymbol{u}^\varepsilon)] - \alpha(\epsilon)\Delta\boldsymbol{u}^\varepsilon - \mathrm{div}(2\nu_0|\boldsymbol{d}(\boldsymbol{u}^\varepsilon)|^{r-2}\boldsymbol{d}(\boldsymbol{u}^\varepsilon)) + \nabla p^\varepsilon = \boldsymbol{f}, \\ \mathrm{div}\boldsymbol{u}^\varepsilon + \varepsilon p^\varepsilon = 0, \\ \boldsymbol{u}^\varepsilon(\boldsymbol{x}, 0) = \boldsymbol{u}_0, \end{cases} \tag{1.2}$$

where $\widetilde{B}(\boldsymbol{u}, \boldsymbol{v}) = (\boldsymbol{u} \cdot \nabla)\boldsymbol{v} + \frac{1}{2}(\mathrm{div}\boldsymbol{u})\boldsymbol{v}$ is the modified bilinear term and $\varepsilon > 0$ is a small penalty parameter and $\boldsymbol{d}(\boldsymbol{u}) = \frac{1}{2}(\nabla\boldsymbol{u} + \nabla\boldsymbol{u}^T)$ denotes the deformation rate tensor. The coefficient $\alpha(\epsilon)$ should be regarded as artificial viscosity such that

$$0 < \alpha(\epsilon) \ll 1 \text{ and } \lim_{\epsilon\to 0}\alpha(\epsilon) = 0. \tag{1.3}$$

The introduction of the coercive term $\alpha(\epsilon)\Delta\boldsymbol{u}^\varepsilon$ in (1.2) provides the stability and smoothness of the system. Note that the synergy between $\alpha(\epsilon)\Delta\boldsymbol{u}^\varepsilon$ and the penalty method is not merely a technical convenience but is an essential coupling for robust non-Newtonian aneurysmal flow simulations. The penalty method effectively manages incompressibility constraints, while the artificial viscosity suppresses the nonlinear instabilities inherent in shear-thinning models. Together, they enable rigorous mathematical analysis and support clinically viable computations by balancing accuracy, efficiency, and numerical robustness. The idea of adding the artificial viscosity originated from the vanishing viscosity method, which has been used to study the existence and uniqueness of partial differential equations [32]. Noting that the "extra diffusion" added in (1.2) makes it easy to carry out the convergence analysis, the numerical simulations of (1.2) might produce more smoothness and better results than solutions obtained by (1.1). On the other hand, it should be observed that $p^\varepsilon$ in (1.2) can be only eliminated to obtain a penalty solution $\boldsymbol{u}^\varepsilon$, which is much easier to solve than the original equations (1.1). The reasons for adopting this approach are well known, namely that it brings computational efficiency and simplification to the problem. The reader can check in many references [33–38] to see the power of the penalty method. Howevwr, the natural question arising from the penalty system is the following: Can the solution $(\boldsymbol{u}^\varepsilon, p^\varepsilon)$ of (1.2) converge to the solution $(\boldsymbol{u}, p)$ of (1.1) as $\varepsilon$ tends to zero? We claim that this is indeed the case and, just to be clear, as far as the authors are aware, it is the first time that such a technique is used in this context.

The main advantages of our proposed schemes are that: (i) overcome the difficulties caused by the incompressibility constraint $\mathrm{div}\boldsymbol{u} = 0$, (ii) it saves central processing unit (CPU) time effectively and has a relatively higher-order precision, and (iii) it guarantees the stability and smoothness of the nonlinear system, easily allowing the consideration of convergence analysis. Unfortunately, to the authors' knowledge, rigorous theoretical justifications for these schemes are not yet available. Therefore, our second task is to provide precise convergence error estimates for the fully discrete forms. The third contribution of this work is to study the flow patterns based on patient-specific geometric models of cerebral aneurysms through segmentation of medical images.

The rest of the paper is organized as follows. In the next section, we recall or prove some notations, present the preliminary results, and introduce the penalized weak formulation. In Section 3, we propose the fully discrete finite element schemes for solving the power-law Navier-Stokes equations. Section 4 we mainly focus on the stability analysis and error estimates for our proposed schemes. In Section 5, numerical examples are performed to confirm the effectiveness of the proposed schemes, and to study

the influence of blood viscosity on hemodynamics in aneurysms. Section 6 is devoted to concluding remarks and a discussion of the ongoing applications.

## 2. Notations and mathematical preliminaries

We first introduce some notations. For $1 \leq r < \infty$, we denote by the Lebesgue space as the usual $L^r(\Omega)$ endowed with the norm $\|\cdot\|_{L^r}$ (except for the $L^2(\Omega)$-norm, which is denoted $\|\cdot\|$). For any non-negative integer $m$ and real number $r \geq 1$, the classical Sobolev space $W^{m,r}(\Omega)$ is defined by

$$W^{m,r}(\Omega) = \{\forall\ v \in L^r(\Omega); \partial^\alpha v \in L^r(\Omega) \text{ for all } |\alpha| \leq m\},$$

is equipped with the semi-norm

$$|v|_{m,r} = (\sum_{|\alpha|=m} \int_\Omega |\partial^\alpha v|^r dx)^{1/r}, \tag{2.1}$$

and the norm

$$\|v\|_{m,r} = (\sum_{l=0}^{m} |\partial^l v|_{l,r}^r)^{1/r}. \tag{2.2}$$

When $r = 2$, $W^{m,r}(\Omega)$ is the Hilbert space $H^m(\Omega)$, for $m = 0$, the space $W^{m,2}(\Omega)$ is usually Lebesgue space $L^2(\Omega)$. $W_0^{m,r}(\Omega)$ consists of the functions of $W^{m,r}(\Omega)$ that vanish on $\partial\Omega$. Let $W^{-m,r'}(\Omega)$ be the topological dual space of $W^{m,r}(\Omega)$, and $\|\cdot\|_{-m,r'}$ is its norm, where $r'$ is the conjugate of $r$ satisfying $1/r+1/r' = 1$, i.e., $r' = r/(r-1)$. $\langle\cdot,\cdot\rangle$ denotes the duality pairing between $W^{m,r}(\Omega)$ and $W^{-m,r'}(\Omega)$ as well as between $L^r(\Omega)$ and $L^{r'}(\Omega)$. The boldface characters $\boldsymbol{W}^{m,r}(\Omega) := [W^{m,r}(\Omega)]^d$ and $\boldsymbol{L}^r(\Omega) := [L^r(\Omega)]^d$ denote the vector quantities. During the course of this study, the following Poincaré-Fredrichs's inequality is needed, which implies that a constant $c > 0$ exist such that

$$\int_\Omega |\boldsymbol{v}|^r dx \leq c \int_\Omega |\nabla \boldsymbol{v}|^r dx \text{ for all } \boldsymbol{v} \in \boldsymbol{W}_0^{m,r}(\Omega), \tag{2.3}$$

which implies that the semi-norm defined in (2.1) is equivalent to the norm (2.2). Also of importance here is Korn's inequality, which statesna constant $c > 0$ exists such that

$$\int_\Omega |\nabla \boldsymbol{v}|^r dx \leq c \int_\Omega |\boldsymbol{d}(\boldsymbol{v})|^r dx \text{ for all } \boldsymbol{v} \in \boldsymbol{W}_0^{m,r}(\Omega). \tag{2.4}$$

For convenience, let us introduce the following space to deal with the pressure:

$$L_0^r(\Omega) := \{q \in L^r(\Omega) : \int_\Omega q dx = 0\},$$

where the zero mean-value condition is added because the pressure is only defined by (1.1). In addition, since div$\boldsymbol{u}$ is an element of $L^r(\Omega)$, it follows that the trial function $q$ must be in $L^{r'}(\Omega)$, and then the pressure must belong to $L^{r'}(\Omega)$. Moreover, the shear tensor term in (1.1) implies that the velocity $\boldsymbol{u}$ and the test function $\boldsymbol{v}$ must belong to $\boldsymbol{W}_0^{m,r}(\Omega)$. Thus, we introduce the following spaces:

$$\boldsymbol{X} := \boldsymbol{W}_0^{m,r}(\Omega) \cap \boldsymbol{L}^2(\Omega),\ Q := L_0^{r'}(\Omega),$$

and the two spaces frequently used in the theory of generalized Navier-Stokes equations are given by

$$\boldsymbol{V} := \{\boldsymbol{v} \in \boldsymbol{X} : \mathrm{div}\boldsymbol{v} = 0\},\ M := L_0^r(\Omega) \cap L_0^{r'}(\Omega),$$

where $M$ is associated with the penalized system, and one observes that the pressure $p$ and the trial function $q$ must be in $M$ because of (1.2).

We now define and introduce some operators associated with the power-law Navier-Stokes equations and their approximations

$$B(\boldsymbol{u}, \boldsymbol{v}) = (\boldsymbol{u} \cdot \nabla)\boldsymbol{v},\ \widetilde{B}(\boldsymbol{u}, \boldsymbol{v}) = (\boldsymbol{u} \cdot \nabla)\boldsymbol{v} + \frac{1}{2}(\mathrm{div}\boldsymbol{u})\boldsymbol{v},\ b(\boldsymbol{u}, \boldsymbol{v}, \boldsymbol{w}) = \langle B(\boldsymbol{u}, \boldsymbol{v}), \boldsymbol{w}\rangle,$$
$$\widetilde{b}(\boldsymbol{u}, \boldsymbol{v}, \boldsymbol{w}) = \langle \widetilde{B}(\boldsymbol{u}, \boldsymbol{v}), \boldsymbol{w}\rangle,\ \langle \mathcal{A}(\boldsymbol{u}), \boldsymbol{v}\rangle = (|\boldsymbol{d}(\boldsymbol{u})|^{r-2}\boldsymbol{d}(\boldsymbol{u}), \boldsymbol{d}(\boldsymbol{v})).$$

It is an easy to verify that

$$b(\boldsymbol{u}, \boldsymbol{v}, \boldsymbol{w}) = -b(\boldsymbol{u}, \boldsymbol{w}, \boldsymbol{v}),\ b(\boldsymbol{u}, \boldsymbol{v}, \boldsymbol{v}) = 0.$$

Therefore, one can readily check that

$$\widetilde{b}(\boldsymbol{u}, \boldsymbol{v}, \boldsymbol{w}) = \frac{1}{2}\{b(\boldsymbol{u}, \boldsymbol{v}, \boldsymbol{w}) - b(\boldsymbol{u}, \boldsymbol{w}, \boldsymbol{v})\},$$

and

$$\widetilde{b}(\boldsymbol{u}, \boldsymbol{v}, \boldsymbol{w}) = -\widetilde{b}(\boldsymbol{u}, \boldsymbol{w}, \boldsymbol{v}),\ \widetilde{b}(\boldsymbol{u}, \boldsymbol{v}, \boldsymbol{v}) = 0. \tag{2.5}$$

Moreover, with the help of integration by parts, Hölder's inequality, and Sobolev inequalities, the following results can be proved, which will be used repeatedly in the sequel [36].

$$\begin{cases} |b(\boldsymbol{u}, \boldsymbol{v}, \boldsymbol{w})| \\ |\tilde{b}(\boldsymbol{u}, \boldsymbol{v}, \boldsymbol{w})| \end{cases} \leq c\|\boldsymbol{u}\|_{1,2}\|\boldsymbol{v}\|_{1,2}\|\boldsymbol{w}\|_{1,2},\ \forall \boldsymbol{u}, \boldsymbol{v}, \boldsymbol{w} \in \boldsymbol{X}, \tag{2.6}$$

and

$$|\tilde{b}(\boldsymbol{u}, \boldsymbol{v}, \boldsymbol{w})| \leq \begin{cases} c\|\boldsymbol{u}\|_{1,2}\|\boldsymbol{v}\|_{2,2}\|\boldsymbol{w}\|, \\ c\|\boldsymbol{u}\|_{2,2}\|\boldsymbol{v}\|_{1,2}\|\boldsymbol{w}\|, \\ c\|\boldsymbol{u}\|_{2,2}\|\boldsymbol{v}\|\|\boldsymbol{w}\|_{1,2}, \\ c\|\boldsymbol{u}\|\|\boldsymbol{v}\|_{2,2}\|\boldsymbol{w}\|_{1,2}, \end{cases} \forall \boldsymbol{u}, \boldsymbol{v}, \boldsymbol{w} \in \boldsymbol{X}, \tag{2.7}$$

where $c$ is a general positive constant depending only on $\Omega$.

With the notations above, the mixed weak formulation of the power-law Navier-Stokes equations (1.1) and the penalized system (1.2) are defined, respectively, as follows. Find $(\boldsymbol{u}, p) \in (\boldsymbol{X}, Q)$ such that for all $(\boldsymbol{v}, q) \in (\boldsymbol{X}, Q)$, we have

$$\begin{cases} \rho(\boldsymbol{u}_t, \boldsymbol{v}) + \rho b(\boldsymbol{u}, \boldsymbol{u}, \boldsymbol{v}) + 2\nu_0\langle \mathcal{A}(\boldsymbol{u}), \boldsymbol{v}\rangle - (\mathrm{div}\boldsymbol{v}, p) = (\boldsymbol{f}, \boldsymbol{v}), \\ (\mathrm{div}\boldsymbol{u}, q) = 0, \end{cases} \tag{2.8}$$

and find $(\boldsymbol{u}^\varepsilon, p^\varepsilon) \in (\boldsymbol{X}, M)$ such that for all $(\boldsymbol{v}, q) \in (\boldsymbol{X}, M)$:

$$\begin{cases} \rho(\boldsymbol{u}_t^\varepsilon, \boldsymbol{v}) + \rho\widetilde{b}(\boldsymbol{u}^\varepsilon, \boldsymbol{u}^\varepsilon, \boldsymbol{v}) + \alpha(\epsilon)(\nabla \boldsymbol{u}^\varepsilon, \nabla \boldsymbol{v}) + 2\nu_0\langle \mathcal{A}(\boldsymbol{u}^\varepsilon), \boldsymbol{v}\rangle - (\mathrm{div}\boldsymbol{v}, p^\varepsilon) = (\boldsymbol{f}, \boldsymbol{v}), \\ (\mathrm{div}\boldsymbol{u}^\varepsilon, q) + \varepsilon(p^\varepsilon, q) = 0, \end{cases} \tag{2.9}$$

with the initial conditions $\boldsymbol{u}(0) = \boldsymbol{u}_0$ and $\boldsymbol{u}^\varepsilon(0) = \boldsymbol{u}_0$, respectively. By eliminating the pressure $p_\varepsilon$, we can get the equivalence formulation of (2.9), which reads as follows: Find $\boldsymbol{u}^\varepsilon \in \boldsymbol{V}$ such that

$$\rho(\frac{\partial \boldsymbol{u}^\varepsilon}{\partial t}, \boldsymbol{v}) + \rho\widetilde{b}(\boldsymbol{u}^\varepsilon, \boldsymbol{u}^\varepsilon, \boldsymbol{v}) + \alpha(\epsilon)(\nabla \boldsymbol{u}^\varepsilon, \nabla \boldsymbol{v}) + 2\nu_0\langle \mathcal{A}(\boldsymbol{u}^\varepsilon), \boldsymbol{v}\rangle + \frac{1}{\varepsilon}(\mathrm{div}\boldsymbol{u}^\varepsilon, \mathrm{div}\boldsymbol{v}) = (\boldsymbol{f}, \boldsymbol{v}). \tag{2.10}$$

We next state some classical results that will be used to performing the error estimates throughout this work.

**Lemma 2.1.** (See [26, 30]) For all $r \in (1, 2]$ and $\boldsymbol{u}, \boldsymbol{v} \in \boldsymbol{X}$, are two constants $\eta = \eta(r, d) > 0$ and $\beta = \beta(r, d) > 0$ such that

$$\langle \mathcal{A}(\boldsymbol{u}) - \mathcal{A}(\boldsymbol{v}), \boldsymbol{u} - \boldsymbol{v}\rangle \geq \eta \|\boldsymbol{u} - \boldsymbol{v}\|_{1,r}^2 (\|\boldsymbol{u}\|_{1,r} + \|\boldsymbol{v}\|_{1,r})^{r-2},$$

and

$$\|\mathcal{A}(\boldsymbol{u}) - \mathcal{A}(\boldsymbol{v})\|_{-1,r'} \leq \beta \|\boldsymbol{u} - \boldsymbol{v}\|_{1,r}^{r-1}.$$

**Lemma 2.2.** (See [32]) Suppose $r \in (1, \infty)$ and $\Omega \subset \mathbb{R}^d$ with $d \geq 1$. Then $\boldsymbol{W}^{1,r}(\Omega) \subset \boldsymbol{L}^2(\Omega)$ is compact for $(2d/(d+2), \infty)$. Moreover, for every $r \in [2d/(d+2), \infty)$, the following holds:

$$\kappa \|\boldsymbol{v}\| \leq \|\boldsymbol{v}\|_{1,r},$$

for all $\boldsymbol{v} \in \boldsymbol{X}$ and $\kappa > 0$ is a generic constant depending on $\Omega, d$, and $r$.

**Lemma 2.3.** For any $r \in (1, \infty)$ and $\Omega \subset \mathbb{R}^d$ that is a bounded domain. Then, there exists a constant $\gamma > 0$ such that

$$0 < \gamma \leq \inf_{q \in Q} \sup_{\boldsymbol{v} \in \boldsymbol{X}} \frac{(\mathrm{div}\boldsymbol{v}, q)}{\|q\|_{0,r'} \|\boldsymbol{v}\|_{1,r}},$$

noting that the above inequality is known as the Ladyzhenskaya-Babuska-Brezzi (LBB) condition [29].

**Lemma 2.4.** (Gronwall's lemma, see [36] ) Let $y(t), h(t), g(t), f(t)$ be non-negative functions satisfying

$$y(t) + \int_0^t h(s)ds \leq y(0) + \int_0^t [g(s)y(s) + f(s)]ds, \ \forall\ 0 \leq t \leq T.$$

We then have

$$y(t) + \int_0^t h(s)ds \leq \exp(\int_0^T g(s)ds)[y(0) + \int_0^t f(s)ds].$$

**Lemma 2.5.** (Discrete Gronwall's lemma, see [36, 39] ) Let $a_n, b_n, d_n, h_n$ be a non-negative series such that

$$a_m + \Delta t \sum_{n=0}^{m} b_n \leq \Delta t \sum_{n=0}^{m} d_n a_n + \Delta t \sum_{n=0}^{m} h_n + M,$$

for all $m \geq 1$ and $M > 0$. Assume that $\Delta t d_n < 1$ for all $n \geq 0$, in which case

$$a_m + \Delta t \sum_{n=0}^{m} b_n \leq \exp(\Delta t \sum_{n=0}^{m} (1 - \Delta t d_n)^{-1} d_n)(\Delta t \sum_{n=1}^{m} h_n + M).$$

Throughout this paper, we need a further assumption on $\Omega$ and the prescribed data for the given problem (1.1).

(**A1**). (see [39, 40]) If we assume that $\Omega$ is smooth and $\boldsymbol{g} \in \boldsymbol{L}^r(\Omega)$, then there is a unique weak solution $(\boldsymbol{v}, q) \in (\boldsymbol{X}, Q)$ to the following steady Stokes system:

$$-\Delta \boldsymbol{v} + \nabla q = \boldsymbol{g},\ \mathrm{div}\boldsymbol{v} = 0 \text{ in } \Omega\ ,\ \boldsymbol{v} = 0 \text{ on } \partial\Omega.$$

Moreover, there is a constant $c > 0$ depending on $\Omega$ such that

$$\|\boldsymbol{v}\|_{2,r} + \|q\|_{1,r} \leq c\|\boldsymbol{g}\|_{\boldsymbol{L}^r},\ 1 < r \leq d^*,$$

where $2 < d^* < 6$.

(**A2**). (Data regularity). We assume that the generalized Navier-Stokes system (1.1) admits a unique solution $(\boldsymbol{u}, p)$. Moreover, assume the regularity on the data satisfying

$$\begin{aligned}&\|\boldsymbol{u}\|_{L^\infty(I;\boldsymbol{W}^{k+1,2}(\Omega))} + \|\boldsymbol{u}_t\|_{L^2(I;\boldsymbol{W}^{k+1,r}(\Omega))} + \|\boldsymbol{u}_{tt}\|_{L^2(I;\boldsymbol{L}^2(\Omega))} + \|\boldsymbol{u}\|_{L^2(I;\boldsymbol{W}^{k+1,r}(\Omega))}\\ &\quad + \|p\|_{L^\infty(I;W^{k,2}(\Omega))} + \|p_t\|_{L^2(I;W^{k,r}(\Omega))} + \|p_{tt}\|_{L^2(I;W^{k,r}(\Omega))} + \|p\|_{L^2(I;W^{k,r}(\Omega))} \leq K,\end{aligned}$$

with $I = (0, T)$, $1 < r < \infty$, and $k = 0, 1, \cdots, n$, where $K > 0$ is a constant. The initial values $\boldsymbol{u}_0$ and the body force $\boldsymbol{f}$ are often assumed to satisfy

$$\|\boldsymbol{u}_0\|_{k,2} + \|\boldsymbol{f}(t)\|_{L^\infty(I;\boldsymbol{L}^r(\Omega))} + \|\boldsymbol{f}_t(t)\|_{L^2(I;\boldsymbol{L}^r(\Omega))} + \|\boldsymbol{f}_{tt}(t)\|_{L^2(I;\boldsymbol{L}^r(\Omega))} \leq K_0.$$

Next, we study the existence and uniqueness of solution to the associated penalized system. Indeed, we can rewrite the penalized formulation (1.2) as an inhomogeneous elliptic system in a divergence form as follows:

$$\begin{cases} -\alpha(\epsilon)\Delta\boldsymbol{u}^\varepsilon - \mathrm{div}(2\nu_0|\boldsymbol{d}(\boldsymbol{u}^\varepsilon)|^{r-2}\boldsymbol{d}(\boldsymbol{u}^\varepsilon)) + \nabla p^\varepsilon = \boldsymbol{g}, \\ \mathrm{div}\boldsymbol{u}^\varepsilon + \varepsilon p^\varepsilon = 0 \text{ in } \Omega, \\ \boldsymbol{u}^\varepsilon = 0 \text{ on } \partial\Omega, \end{cases} \tag{2.11}$$

where we should write $\boldsymbol{g} = \boldsymbol{f} - \rho[\boldsymbol{u}_t^\varepsilon + (\boldsymbol{u}^\varepsilon \cdot \nabla)\boldsymbol{u}^\varepsilon]$ in (1.2). The mixed weak formulation of (2.11) ia as follows: Find $(\boldsymbol{u}^\varepsilon, p^\varepsilon) \in \boldsymbol{X} \times M$ such that

$$\begin{cases} \alpha(\epsilon)(\nabla\boldsymbol{u}^\varepsilon, \nabla\boldsymbol{v}) + 2\nu_0\langle\mathcal{A}(\boldsymbol{u}^\varepsilon), \boldsymbol{v}\rangle - (p^\varepsilon, \mathrm{div}\boldsymbol{v}) = (\boldsymbol{g}, \boldsymbol{v}),\ \forall\ \boldsymbol{v} \in \boldsymbol{X}, \\ (\mathrm{div}\boldsymbol{u}^\varepsilon, q) + \varepsilon(p^\varepsilon, q) = 0,\ \forall\ q \in M. \end{cases} \tag{2.12}$$

Following what we did earlier, we need to find $\boldsymbol{u}^\varepsilon \in \boldsymbol{V}$ such that

$$\alpha(\epsilon)(\nabla\boldsymbol{u}^\varepsilon, \nabla\boldsymbol{v}) + 2\nu_0\langle\mathcal{A}(\boldsymbol{u}^\varepsilon), \boldsymbol{v}\rangle + \frac{1}{\varepsilon}(\mathrm{div}\boldsymbol{u}^\varepsilon, \mathrm{div}\boldsymbol{v}) = (\boldsymbol{g}, \boldsymbol{v}), \tag{2.13}$$

for $\forall\ \boldsymbol{v} \in \boldsymbol{V}$. It turns out that (2.13) can be restated as a minimization problem; to be more precise, we define the functional $J_\varepsilon : \boldsymbol{V} \to \mathbb{R}$ given by

$$J_\varepsilon(\boldsymbol{w}) = \frac{\alpha(\epsilon)}{2}\|\nabla \boldsymbol{w}\|^2 + \frac{2\nu_0}{r}\|\boldsymbol{d}(\boldsymbol{w})\|_{0,r}^r + \frac{1}{2\varepsilon}\|\mathrm{div}\boldsymbol{w}\|^2 - (\boldsymbol{g}, \boldsymbol{w}),\ \forall \boldsymbol{w} \in \boldsymbol{V}. \tag{2.14}$$

For $\forall\ t \in [0, 1]$ and $\boldsymbol{u}, \boldsymbol{v} \in \boldsymbol{V}$, it is a straightforward calculation to check that $J_\varepsilon$ is Gâteaux differentiable on $\boldsymbol{V}$, that is

$$\begin{aligned}
\langle J_\varepsilon'(\boldsymbol{u}), \boldsymbol{v}\rangle &= \lim_{t\to 0}\frac{d}{dt}J_\varepsilon(\boldsymbol{u} + t\boldsymbol{v}) \\
&= \lim_{t\to 0}\int_\Omega [\alpha(\epsilon)\nabla(\boldsymbol{u} + t\boldsymbol{v}) \cdot \nabla \boldsymbol{v} + 2\nu_0|\boldsymbol{d}(\boldsymbol{u} + t\boldsymbol{v})|^{r-2}\boldsymbol{d}(\boldsymbol{u} + t\boldsymbol{v}) \cdot \boldsymbol{d}(\boldsymbol{v}) \\
&\quad + \frac{1}{\varepsilon}\mathrm{div}(\boldsymbol{u} + t\boldsymbol{v}) \cdot \mathrm{div}\boldsymbol{v} - \boldsymbol{g} \cdot \boldsymbol{v}]dx \\
&= \int_\Omega [\alpha(\epsilon)\nabla \boldsymbol{u} \cdot \nabla \boldsymbol{v} + 2\nu_0|\boldsymbol{d}(\boldsymbol{u})|^{r-2}\boldsymbol{d}(\boldsymbol{u}) \cdot \boldsymbol{d}(\boldsymbol{v}) + \frac{1}{\varepsilon}(\mathrm{div}\boldsymbol{u}) \cdot (\mathrm{div}\boldsymbol{v}) - \boldsymbol{g} \cdot \boldsymbol{v}]dx \\
&:= \langle \mathcal{N}_\varepsilon(\boldsymbol{u}), \boldsymbol{v}\rangle - (\boldsymbol{g}, \boldsymbol{v}),
\end{aligned} \tag{2.15}$$

where $\langle \mathcal{N}_\varepsilon(\boldsymbol{u}), \boldsymbol{v}\rangle = \alpha(\epsilon)(\nabla \boldsymbol{u}, \nabla \boldsymbol{v}) + 2\nu_0\langle \mathcal{A}(\boldsymbol{u}), \boldsymbol{v}\rangle + \frac{1}{\varepsilon}(\mathrm{div}\boldsymbol{u}, \mathrm{div}\boldsymbol{v})$. One readily observes that the solution of the variational formulation (2.12) is equivalent to the following optimization problem

$$\begin{cases} \text{Find } \boldsymbol{u} \in \boldsymbol{V} \text{ such that} \\ J_\varepsilon(\boldsymbol{u}) \le J_\varepsilon(\boldsymbol{v}) \text{ for all } \boldsymbol{v} \in \boldsymbol{V}. \end{cases} \tag{2.16}$$

Firstly, observing that $|(\boldsymbol{g}, \boldsymbol{v})| \le \|\boldsymbol{g}\|_{0,r'}\|\boldsymbol{v}\|_{0,r} \le c_1\|\boldsymbol{g}\|_{0,r'}\|\boldsymbol{v}\|_{1,r}$; together with (2.4), we have

$$J_\varepsilon(\boldsymbol{v}) \ge \frac{\alpha(\epsilon)}{2}\|\nabla \boldsymbol{v}\|^2 + \frac{2c^{-1}\nu_0}{r}\|\nabla \boldsymbol{v}\|_{0,r}^r + \frac{1}{2\varepsilon}\|\mathrm{div}\boldsymbol{v}\|^2 - c_1\|\boldsymbol{g}\|_{0,r'}\|\boldsymbol{v}\|_{1,r}.$$

It is easy to check that

$$\lim_{\|\boldsymbol{v}\|_{1,r}\to\infty} J_\varepsilon(\boldsymbol{v}) = \infty,$$

which implies that $J_\varepsilon(\cdot)$ is coercive on $\boldsymbol{V}$.

Secondly, by Lemma 2.1 and (2.15), we have

$$\begin{aligned}
&\langle J_\varepsilon'(\boldsymbol{u}) - J_\varepsilon'(\boldsymbol{v}), \boldsymbol{u} - \boldsymbol{v}\rangle \\
&= \langle \mathcal{N}_\varepsilon(\boldsymbol{u}) - \mathcal{N}_\varepsilon(\boldsymbol{v}), \boldsymbol{u} - \boldsymbol{v}\rangle \\
&= \alpha(\epsilon)(\nabla(\boldsymbol{u} - \boldsymbol{v}), \nabla(\boldsymbol{u} - \boldsymbol{v})) + 2\nu_0\langle \mathcal{A}(\boldsymbol{u}) - \mathcal{A}(\boldsymbol{v}), \boldsymbol{u} - \boldsymbol{v}\rangle + \frac{1}{\varepsilon}(\mathrm{div}(\boldsymbol{u} - \boldsymbol{v}), \mathrm{div}(\boldsymbol{u} - \boldsymbol{v})) \\
&\ge (\alpha(\epsilon) + \frac{1}{\varepsilon})\|\mathrm{div}(\boldsymbol{u} - \boldsymbol{v})\|^2 + 2\nu_0\eta(\|\boldsymbol{u}\|_{1,r} + \|\boldsymbol{v}\|_{1,r})^{r-2}\|\nabla(\boldsymbol{u} - \boldsymbol{v})\|_{0,r}^2 \\
&\ge C(\|\mathrm{div}(\boldsymbol{u} - \boldsymbol{v})\|^2 + \|\nabla(\boldsymbol{u} - \boldsymbol{v})\|_{0,r}^2),
\end{aligned}$$

which implies that $J_\varepsilon(\cdot)$ is strictly convex. The existence and uniqueness of the solution to the optimization problem (2.16) easily follows. Consequently, the problem (2.12) has a unique weak solution. Since

the existence of $p^\varepsilon$ is simple to check, we are now in the position to prove the uniqueness of $p^\varepsilon$. We know that $\boldsymbol{u}^\varepsilon$ is unique, we assume that $(\boldsymbol{u}^\varepsilon, p_1^\varepsilon)$ and $(\boldsymbol{u}^\varepsilon, p_2^\varepsilon)$ are two solutions satisfying (2.12), in which case we have

$$\varepsilon(p_1^\varepsilon - p_2^\varepsilon, \mathrm{div}\boldsymbol{v}) = 0. \tag{2.17}$$

By picking $q = p_1^\varepsilon - p_2^\varepsilon$ in the inf-sup condition, one obtains

$$\sup_{\boldsymbol{v}\in \boldsymbol{W}_0^{1,r}(\Omega)} \frac{(\mathrm{div}\boldsymbol{v}, p_1^\varepsilon - p_2^\varepsilon)}{\|\boldsymbol{v}\|_{1,r}} \geq \gamma \|p_1^\varepsilon - p_2^\varepsilon\|_{0,r'}. \tag{2.18}$$

Thus, (2.17) and (2.18) imply that $\gamma\|p_1^\varepsilon - p_2^\varepsilon\|_{0,r'} \leq 0$, which leads to the uniqueness of $p^\varepsilon$. Therefore, we have proved that there is a unique solution $(\boldsymbol{u}^\varepsilon, p^\varepsilon)$ to the mixed weak formulation of the steady penalized problem (2.12).

Finally, under some suitable conditions associated with $\boldsymbol{g}$ as similarly shown in (**A2**), we can obtain the existence and uniqueness of solution to the penalized system (1.2).

## 3. Artificial viscosity penalty finite element method

In this section, we consider the fully discrete finite element approximation of (1.1) based on the penalized system (1.2). The main purpose for introducing the artificial viscosity penalized system (1.2) is to alleviate some difficulties related to the numerical solution of (1.1). Before going to the numerical investigations, we start by proving the strong convergence of $(\boldsymbol{u}^\varepsilon, p^\varepsilon)$ to $(\boldsymbol{u}, p)$ as $\varepsilon \to 0$ and $\epsilon \to 0$, which is essential for the rest of the paper. To simplify the presentation, we need more regularity results on the solution of the penalized system (1.2) as shown in Hypothesis (**A1**) and (**A2**).

**Theorem 3.1.** Let the assumptions (**A1**) and (**A2**) be valid. Let $(\boldsymbol{u}, p)$ solve (1.1) and $(\boldsymbol{u}^\varepsilon, p^\varepsilon)$ solve (1.2). We then have

$$\rho\|\boldsymbol{u} - \boldsymbol{u}^\varepsilon\|^2 + \int_0^t \{\alpha(\epsilon)\|\nabla(\boldsymbol{u} - \boldsymbol{u}^\varepsilon)\|^2 + \nu_0\|\boldsymbol{u} - \boldsymbol{u}^\varepsilon\|_{1,r}^2 + \varepsilon\|p - p^\varepsilon\|^2\}ds \leq C(\varepsilon + \alpha(\epsilon)),$$

where $C > 0$ is some constant that is independent of $\varepsilon$.

**Proof.** Let the penalty errors be $\boldsymbol{e} = \boldsymbol{u} - \boldsymbol{u}^\varepsilon$ and $\phi = p - p^\varepsilon$, then by subtracting (2.8) from (2.9), we obtain

$$\begin{cases} \rho(\boldsymbol{e}_t, \boldsymbol{v}) + \rho[b(\boldsymbol{u}, \boldsymbol{u}, \boldsymbol{v}) - \widetilde{b}(\boldsymbol{u}^\varepsilon, \boldsymbol{u}^\varepsilon, \boldsymbol{v})] - \alpha(\epsilon)(\nabla\boldsymbol{u}^\varepsilon, \nabla\boldsymbol{v}) \\ \qquad + 2\nu_0\langle\mathcal{A}(\boldsymbol{u}) - \mathcal{A}(\boldsymbol{u}^\varepsilon), \boldsymbol{v}\rangle - (\mathrm{div}\boldsymbol{v}, \phi) = 0, \\ (\mathrm{div}\boldsymbol{e}, q) + \varepsilon(\phi, q) = \varepsilon(p, q). \end{cases} \tag{3.1}$$

Setting $\boldsymbol{v} = \boldsymbol{e}$ and $q = \phi$ in (3.1), and putting together the results, we get

$$\begin{aligned} &\frac{\rho}{2}\frac{d}{dt}\|\boldsymbol{e}\|^2 + 2\nu_0\langle\mathcal{A}(\boldsymbol{u}) - \mathcal{A}(\boldsymbol{u}^\varepsilon), \boldsymbol{e}\rangle + \varepsilon\|\phi\|^2 + \alpha(\epsilon)\|\nabla\boldsymbol{e}\|^2 \\ &\quad = \varepsilon(p, \phi) + \alpha(\epsilon)(\nabla\boldsymbol{u}, \nabla\boldsymbol{e}) - \rho[b(\boldsymbol{u}, \boldsymbol{u}, \boldsymbol{e}) - \widetilde{b}(\boldsymbol{u}^\varepsilon, \boldsymbol{u}^\varepsilon, \boldsymbol{e})]. \end{aligned} \tag{3.2}$$

According to Lemma 2.1 and (**A2**), we have

$$2\nu_0\langle\mathcal{A}(\boldsymbol{u}) - \mathcal{A}(\boldsymbol{u}^\varepsilon), \boldsymbol{e}\rangle \geq 2\nu_0\eta\|\boldsymbol{e}\|_{1,r}^2(\|\boldsymbol{u}\|_{1,r} + \|\boldsymbol{u}^\varepsilon\|_{1,r})^{r-2} \geq \frac{\lambda_0}{2}\|\boldsymbol{e}\|_{1,r}^2, \tag{3.3}$$

where we choose $\lambda_0 = 2^r \nu_0 \eta K^{r-2} > 0$. Making use of Young's inequality, we obtain

$$\varepsilon(p, \phi) \leq \frac{\varepsilon}{2}\|p\|^2 + \frac{\varepsilon}{2}\|\phi\|^2, \tag{3.4}$$

and

$$\alpha(\epsilon)(\nabla \boldsymbol{u}, \nabla \boldsymbol{e}) \leq \frac{\alpha(\epsilon)}{4}\|\nabla \boldsymbol{e}\|^2 + \alpha(\epsilon)\|\nabla \boldsymbol{u}\|^2. \tag{3.5}$$

Through application of the properties of the form $b$ and Young's inequality, we have

$$\begin{aligned} |b(\boldsymbol{u}, \boldsymbol{u}, \boldsymbol{e}) - \widetilde{b}(\boldsymbol{u}^\varepsilon, \boldsymbol{u}^\varepsilon, \boldsymbol{e})| &= |b(\boldsymbol{u}, \boldsymbol{u} - \boldsymbol{u}^\varepsilon, \boldsymbol{e}) + b(\boldsymbol{u} - \boldsymbol{u}^\varepsilon, \boldsymbol{u}^\varepsilon, \boldsymbol{e})| \\ &\leq c\|\nabla \boldsymbol{e}\|(\|\Delta \boldsymbol{u}\| + \|\Delta \boldsymbol{u}^\varepsilon\|)\|\boldsymbol{e}\| \\ &\leq \frac{\alpha(\epsilon)}{4}\|\nabla \boldsymbol{e}\|^2 + \frac{C}{2\alpha(\epsilon)}\|\boldsymbol{e}\|^2. \end{aligned} \tag{3.6}$$

Combining the estimates (3.2)–(3.6) with (3.1) yields

$$\begin{aligned} &\frac{d}{dt}\|\boldsymbol{e}\|^2 + \frac{1}{\rho}[\alpha(\epsilon)\|\nabla \boldsymbol{e}\|^2 + \nu_0\|\boldsymbol{e}\|_{1,r}^2 + \varepsilon\|\phi\|^2] \\ &\quad \leq \frac{\varepsilon}{\rho}\|p\|^2 + \frac{c^\dagger}{\rho}\|\boldsymbol{e}\|^2 + \frac{2\alpha(\epsilon)}{\rho}\|\nabla \boldsymbol{u}\|^2. \end{aligned} \tag{3.7}$$

Integrating the inequality (3.7) from 0 to $t$, since $\boldsymbol{e}(0) = 0$, we obtain

$$\begin{aligned} &\|\boldsymbol{e}(t)\|^2 + \frac{1}{\rho}\int_0^t \{\alpha(\epsilon)\|\nabla \boldsymbol{e}(s)\|^2 + \nu_0\|\boldsymbol{e}(s)\|_{1,r}^2 + \varepsilon\|\phi(s)\|^2\} ds \\ &\quad \leq \frac{\varepsilon}{\rho}\int_0^t \|p(s)\|^2 ds + \frac{c^\dagger}{\rho}\int_0^t \|\boldsymbol{e}(s)\|^2 ds + \frac{2\alpha(\epsilon)}{\rho}\int_0^t \|\nabla \boldsymbol{u}(s)\|^2 ds. \end{aligned}$$

Using Lemma 2.4 and assumptions (**A1**) and (**A2**), provided that $p$ is contained in $L^\infty(I; L^2(\Omega))$ and $\boldsymbol{u}$ in $L^2(I; \boldsymbol{W}^{k+1,2}(\Omega))$, we deduce the following result:

$$\|\boldsymbol{u} - \boldsymbol{u}^\varepsilon\|^2 + \frac{1}{\rho}\int_0^t \{\alpha(\epsilon)\|\nabla(\boldsymbol{u} - \boldsymbol{u}^\varepsilon)\|^2 + \nu_0\|\boldsymbol{u} - \boldsymbol{u}^\varepsilon\|_{1,r}^2 + \varepsilon\|p - p^\varepsilon\|^2\} ds \leq C(\varepsilon + \alpha(\epsilon)).$$

**Remark 3.1.** Note that the convergence order with respect to $\varepsilon$ for the pressure term in Theorem 3.1 is not optimal, but we can prove that the convergence order of $p$ is equal to $1/2$ about $\varepsilon$. Due to the page limit, we omit the proof here, but the interested readers can refer to [36, 37].

We now discretize the penalized system (1.2) instead of the original problem (1.1). Let $\mathcal{T}_H$ be a family of triangulations of $\Omega$ and let $\mathcal{T}_h$ be a refinement of $\mathcal{T}_H$. We assume that $\boldsymbol{X}_h \subset \boldsymbol{X}$ and $Q_h \subset Q$ are two conforming finite element spaces defined on a fine mesh $\mathcal{T}_h$. Let $h_K$ denote the diameter of a cell $K \in \mathcal{T}_h$. The mesh size $h \in (0, 1)$ denotes the maximum diameter of all cells $K$ on $\mathcal{T}_h$. We also introduce a coarse or large-scale space $\mathcal{M}_h$ defined on a regular mesh $\mathcal{T}_H$, with the maximum element diameter $H$. The choice of $\mathcal{M}_h$, which we will use, is defined on the same grids as $(\boldsymbol{X}_h, Q_h)$, but use the lower degree polynomials.

We state some useful approximation results [41]. For any integers $n, m \geq 1$ and $r \in [1, \infty)$, the following inequalities hold.

**(B1)** Let $\Pi_h : \boldsymbol{X} \to \boldsymbol{X}_h$ be a linear operator, such that for $k = 0, 1, \cdots, n$

$$\|\boldsymbol{v} - \Pi_h \boldsymbol{v}\|_{0,r} + h\|\boldsymbol{v} - \Pi_h \boldsymbol{v}\|_{1,r} \le Ch^{k+1}\|\boldsymbol{v}\|_{k+1,r}, \ \forall \boldsymbol{v} \in \boldsymbol{W}_0^{k,r}(\Omega) \cap \boldsymbol{W}^{k+1,r}(\Omega), \tag{3.8}$$

and we also assume that

$$(\boldsymbol{u} - \Pi_h \boldsymbol{u}, \boldsymbol{v}) = 0, \ \forall \boldsymbol{v} \in \boldsymbol{X}_h. \tag{3.9}$$

**(B2)** Let $\varrho_h : \boldsymbol{L}^r(\Omega) \to Q_h$ be a linear operator, such that for $k = 0, 1, \cdots, m$

$$\|q - \varrho_h q\|_{\boldsymbol{L}^r} \le Ch^k \|q\|_{k,r}, \ \forall q \in W^{k,r}(\Omega). \tag{3.10}$$

where $C$ is a positive constant that is independent of $h$.

**(B3)** The spaces $\boldsymbol{X}_h$ and $Q_h$ satisfy the discrete LBB inf-sup condition. There is a constant $\gamma > 0$ independent of $h$ such that

$$0 < \gamma \le \inf_{q_h \in Q_h} \sup_{\boldsymbol{v}_h \in \boldsymbol{X}_h} \frac{(\mathrm{div}\boldsymbol{v}_h, q_h)}{\|q_h\|_{0,r'}\|\boldsymbol{v}_h\|_{1,r}}. \tag{3.11}$$

**(B4)** For $\forall \boldsymbol{v}_h \in \boldsymbol{X}_h$, the inverse inequality holds

$$\|\nabla \boldsymbol{v}_h\| \le ch^{-1}\|\boldsymbol{v}_h\|, \tag{3.12}$$

where $c > 0$ is a constant that does not depend on $h$.

**(B5)** Let the projection $P_H : \boldsymbol{L}^2(\Omega) \to \mathcal{M}_h$ be defined by

$$(\psi - P_H \psi, \phi_H) = 0, \ \forall \phi_H \in \mathcal{M}_h. \tag{3.13}$$

Then, the approximation on coarse mesh space $\mathcal{M}_h$ is given by

$$\|\psi - P_H \psi\| \le CH^k \|\psi\|_{k+1,2}, \ \forall \psi \in W^{k+1,2}(\Omega), \tag{3.14}$$

where $C > 0$ is a constant that is independent of $H$.

Let $N \in \mathbb{N}$ be a positive integer and define the uniform mesh size $\tau = T/N$ with $t_n = n\tau$ for $n = 0, 1, \cdots, N$. We then look for an approximation to $(\boldsymbol{u}(t), p(t))$ at each time level $t^n$, and let $(\boldsymbol{u}_h^n, p_h^n)$ denote the corresponding finite dimensional functions. To start with, a simple and common fully discrete FEM is used to solve (1.1) directly.

**Algorithm 3.1.** Find $(\boldsymbol{u}_h^n, p_h^n) \in \boldsymbol{X}_h \times Q_h$ such that for all $(\boldsymbol{v}_h, q_h) \in \boldsymbol{X}_h \times Q_h$, we have

$$\begin{cases} \rho(\frac{\boldsymbol{u}_h^n - \boldsymbol{u}_h^{n-1}}{\tau}, \boldsymbol{v}_h) + \rho b(\boldsymbol{u}_h^n, \boldsymbol{u}_h^n, \boldsymbol{v}_h) + 2\nu_0\langle \mathcal{A}(\boldsymbol{u}_h^n), \boldsymbol{v}_h\rangle - (p_h^n, \mathrm{div}\boldsymbol{v}_h) = (\boldsymbol{f}(t^n), \boldsymbol{v}_h), \\ (\mathrm{div}\boldsymbol{u}_h^n, q_h) = 0. \end{cases} \tag{3.15}$$

We notice that the prior estimate of this scheme is hard to obtain directly, and the proofs of stability and convergence are also difficult because of the strong nonlinearity and the viscosity loses regularity close to shocks and sharp discontinuities. Therefore, the numerical analysis of the scheme (3.15) will not be addressed in this paper.

Next, we consider the time discretization of (1.1) based on the penalized system (1.2). The backward Euler scheme and penalty projection scheme are proposed for the temporal approximation. Then the fully discrete versions of (1.2) are given as follows.

**Algorithm 3.2.** Find $(\boldsymbol{u}_h^{\varepsilon,n}, p_h^{\varepsilon,n}, S_H^n) \in \boldsymbol{X}_h \times Q_h \times \mathcal{M}_H$ such that for all $(\boldsymbol{v}_h, q_h, \phi_H) \in \boldsymbol{X}_h \times Q_h \times \mathcal{M}_H$, then following hold:

$$\begin{cases} \rho(\frac{\boldsymbol{u}_h^{\varepsilon,n}-\boldsymbol{u}_h^{\varepsilon,n-1}}{\tau}, \boldsymbol{v}_h) + \rho\widetilde{b}(\boldsymbol{u}_h^{\varepsilon,n}, \boldsymbol{u}_h^{\varepsilon,n}, \boldsymbol{v}_h) + 2\nu_0\langle\mathcal{A}(\boldsymbol{u}_h^{\varepsilon,n}), \boldsymbol{v}_h\rangle - (p_h^{\varepsilon,n}, \mathrm{div}\boldsymbol{v}_h) \\ \quad + \frac{\alpha(\epsilon)}{2}(\nabla\boldsymbol{u}_h^{\varepsilon,n} + S_H^n, \nabla\boldsymbol{v}_h) = (\boldsymbol{f}(t^n), \boldsymbol{v}_h), \\ (S_H^n - \nabla\boldsymbol{u}_h^{\varepsilon,n-1}, \phi_H) = 0, \\ (\mathrm{div}\boldsymbol{u}_h^{\varepsilon,n}, q_h) + \varepsilon(p_h^{\varepsilon,n}, q_h) = 0, \end{cases} \tag{3.16}$$

where the user-selected artificial viscosity parameter $\alpha(\epsilon)$ is proposed as the $O(h^2)$ constant. From the last two equations in (3.16), one can write $S_H^n = P_H\nabla\boldsymbol{u}_h^{\varepsilon,n-1}$ and $p_h^{\varepsilon,n} = -\frac{1}{\varepsilon}\mathrm{div}\boldsymbol{u}_h^{\varepsilon,n}$, and then the equivalence formulation of (3.16) can also be rewritten as

$$\begin{aligned} &\rho(\frac{\boldsymbol{u}_h^{\varepsilon,n}-\boldsymbol{u}_h^{\varepsilon,n-1}}{\tau}, \boldsymbol{v}_h) + \rho\widetilde{b}(\boldsymbol{u}_h^{\varepsilon,n}, \boldsymbol{u}_h^{\varepsilon,n}, \boldsymbol{v}_h) + 2\nu_0\langle\mathcal{A}(\boldsymbol{u}_h^{\varepsilon,n}), \boldsymbol{v}_h\rangle + \frac{1}{\varepsilon}(\mathrm{div}\boldsymbol{u}_h^{\varepsilon,n}, \mathrm{div}\boldsymbol{v}_h) \\ &\quad + \frac{\alpha(\epsilon)}{2}(\nabla\boldsymbol{u}_h^{\varepsilon,n}, \nabla\boldsymbol{v}_h) + \frac{\alpha(\epsilon)}{2}(P_H\nabla\boldsymbol{u}_h^{\varepsilon,n-1}, \nabla\boldsymbol{v}_h) = (\boldsymbol{f}(t^n), \boldsymbol{v}_h). \end{aligned} \tag{3.17}$$

**Algorithm 3.3.** Assume that $\boldsymbol{u}_h^{\varepsilon,0} = \tilde{\boldsymbol{u}}_h^{\varepsilon,0} = \boldsymbol{u}_{h0}$. Find $(\boldsymbol{u}_h^{\varepsilon,n}, p_h^{\varepsilon,n}, S_H^n) \in \boldsymbol{X}_h \times Q_h \times \mathcal{M}_H$ such that for all $(\boldsymbol{v}_h, q_h, \phi_H) \in \boldsymbol{X}_h \times Q_h \times \mathcal{M}_H$, then following hold:

• *Penalization*.

$$\begin{cases} \rho(\frac{\tilde{\boldsymbol{u}}_h^{\varepsilon,n}-\boldsymbol{u}_h^{\varepsilon,n-1}}{\tau}, \boldsymbol{v}_h) + \rho\widetilde{b}(\tilde{\boldsymbol{u}}_h^{\varepsilon,n}, \tilde{\boldsymbol{u}}_h^{\varepsilon,n}, \boldsymbol{v}_h) + 2\nu_0\langle\mathcal{A}(\tilde{\boldsymbol{u}}_h^{\varepsilon,n}), \boldsymbol{v}_h\rangle - (\tilde{p}_h^{\varepsilon,n}, \mathrm{div}\boldsymbol{v}_h) \\ \quad + (\nabla\phi_h^{\varepsilon,n-1}, \boldsymbol{v}_h) + \frac{\alpha(\epsilon)}{2}(\nabla\tilde{\boldsymbol{u}}_h^{\varepsilon,n} + S_H^n, \nabla\boldsymbol{v}_h) = (\boldsymbol{f}(t^n), \boldsymbol{v}_h), \\ (S_H^n - \tilde{\boldsymbol{u}}_h^{\varepsilon,n-1}, \phi_H) = 0, \\ (\mathrm{div}\tilde{\boldsymbol{u}}_h^{\varepsilon,n}, q_h) + \varepsilon(\tilde{p}_h^{\varepsilon,n}, q_h) = 0. \end{cases} \tag{3.18}$$

Given $(\tilde{\boldsymbol{u}}_h^{\varepsilon,n}, \tilde{p}_h^{\varepsilon,n})$, find $(\boldsymbol{u}_h^{\varepsilon,n}, p_h^{\varepsilon,n})$ such that

• *Projection*.

$$\begin{cases} \rho(\frac{\boldsymbol{u}_h^{\varepsilon,n}-\tilde{\boldsymbol{u}}_h^{\varepsilon,n}}{\tau}, \boldsymbol{v}_h) + \delta(\nabla(\phi_h^{\varepsilon,n} - \phi_h^{\varepsilon,n-1}), \boldsymbol{v}_h) = 0, \\ (\mathrm{div}\boldsymbol{u}_h^{\varepsilon,n}, q_h) = 0. \end{cases} \tag{3.19}$$

In addition, the discrete pressure $p_h^{\varepsilon,n}$ can be computed via

$$p_h^{\varepsilon,n} = \tilde{p}_h^{\varepsilon,n} + \phi_h^{\varepsilon,n} + \delta(\phi_h^{\varepsilon,n} - \phi_h^{\varepsilon,n-1}), \tag{3.20}$$

where $\delta > 1$ can be any constant.

**Remark 3.2.** Both the pressure correction projection method and classical projection schemes (e.g., Chorin Temam) use a fractional-step strategy to solve incompressible flow problems. While classical

methods decompose the solution into simpler substeps, they often suffer from numerical artifacts such as spurious boundary layers and challenges in enforcing pressure boundary conditions. The pressure-correction projection method preserves this stepwise framework but introduces a key innovation: An iterative pressure correction term. This enhancement not only improves the temporal accuracy but also enhances numerical stability, effectively overcoming the limitations of classical approaches. Therefore, it can be regarded as a refined extension of traditional projection methods.

In the next section, we focus on the numerical analysis of the fully discrete scheme (3.16) and penalty projection scheme (3.18)–(3.20) for the penalized system (1.2).

## 4. Stability analysis and error estimates

In this section, let us concentrate our attention on the stability and convergence analysis of Algorithms 3.2 and 3.3 presented in the previous section. Under some suitable assumptions on the data, we are now in a position to state the main results.

### *4.1. Numerical analysis of Algorithm 3.2*

**Theorem 4.1.** Assume that (**A1**) and (**A2**) hold. Then, the solution $(\boldsymbol{u}_h^{\varepsilon,n}, p_h^{\varepsilon,n})$ to the fully discrete formulation (3.16) is unconditionally stable. More precisely, we have

$$\max_{1\le m\le N}\{\|\boldsymbol{u}_h^{\varepsilon,m}\|^2+\frac{\alpha(\epsilon)\tau}{2\rho}\|\nabla\boldsymbol{u}_h^{\varepsilon,m}\|^2\}+\sum_{n=1}^{N}\|\boldsymbol{u}_h^{\varepsilon,n}-\boldsymbol{u}_h^{\varepsilon,n-1}\|^2+\frac{4\nu_0\tau}{\rho}\sum_{n=1}^{N}\|\boldsymbol{d}(\boldsymbol{u}_h^{\varepsilon,n})\|_{0,r}^r$$
$$+\frac{2\tau}{\rho\varepsilon}\sum_{n=1}^{N}\|\mathrm{div}\boldsymbol{u}_h^{\varepsilon,n}\|^2\le C(\|\boldsymbol{u}_h^{\varepsilon,0}\|^2+\|\nabla\boldsymbol{u}_h^{\varepsilon,0}\|^2+\sum_{n=1}^{N}\|\boldsymbol{f}(t^n)\|^2), \tag{4.1}$$

$$\frac{2\varepsilon\tau}{\rho}\sum_{n=1}^{N}\|p_h^{\varepsilon,n}\|^2\le C(\|\boldsymbol{u}_h^{\varepsilon,0}\|^2+\|\nabla\boldsymbol{u}_h^{\varepsilon,0}\|^2+\sum_{n=1}^{N}\|\boldsymbol{f}(t^n)\|^2), \tag{4.2}$$

where $C>0$ is a generic constant.

**Proof.** To start the proof, we set $\boldsymbol{v}_h=\boldsymbol{u}_h^{\varepsilon,n}$ in $(3.16)_1$ and $q_h=\mathrm{div}\boldsymbol{u}_h^{\varepsilon,n}$ in $(3.16)_3$, adding the results, and vanishing the skew-symmetric trilinear term to obtain

$$\rho(\frac{\boldsymbol{u}_h^{\varepsilon,n}-\boldsymbol{u}_h^{\varepsilon,n-1}}{\tau},\boldsymbol{u}_h^{\varepsilon,n})+2\nu_0\|\boldsymbol{d}(\boldsymbol{u}_h^{\varepsilon,n})\|_{0,r}^r+\frac{1}{\varepsilon}\|\mathrm{div}\boldsymbol{u}_h^{\varepsilon,n}\|^2+\frac{\alpha(\epsilon)}{2}\|\nabla\boldsymbol{u}_h^{\varepsilon,n}\|^2$$
$$=(\boldsymbol{f}(t^n),\boldsymbol{u}_h^{\varepsilon,n})-\frac{\alpha(\epsilon)}{2}(S_H^n,\nabla\boldsymbol{u}_h^{\varepsilon,n}). \tag{4.3}$$

Using the algebraic identity

$$2(a-b)a=a^2-b^2+(a-b)^2 \tag{4.4}$$

for the first term on the left-hand side of (4.3), we obtain

$$\frac{\rho}{2\tau}(\|\boldsymbol{u}_h^{\varepsilon,n}\|^2-\|\boldsymbol{u}_h^{\varepsilon,n-1}\|^2)+\frac{\rho}{2\tau}\|\boldsymbol{u}_h^{\varepsilon,n}-\boldsymbol{u}_h^{\varepsilon,n-1}\|^2+2\nu_0\|\boldsymbol{d}(\boldsymbol{u}_h^{\varepsilon,n})\|_{0,r}^r+\frac{1}{\varepsilon}\|\mathrm{div}\boldsymbol{u}_h^{\varepsilon,n}\|^2$$

$$+\frac{\alpha(\epsilon)}{2}\|\nabla \boldsymbol{u}_h^{\varepsilon,n}\|^2=(\boldsymbol{f}(t^n),\boldsymbol{u}_h^{\varepsilon,n})-\frac{\alpha(\epsilon)}{2}(S_H^n,\nabla \boldsymbol{u}_h^{\varepsilon,n}). \tag{4.5}$$

The application of the Cauchy-Schwarz inequality and Young's inequality on the right-hand terms of Eq (4.5) gives

$$\begin{aligned}&\frac{\rho}{2\tau}(\|\boldsymbol{u}_h^{\varepsilon,n}\|^2-\|\boldsymbol{u}_h^{\varepsilon,n-1}\|^2)+\frac{\rho}{2\tau}\|\boldsymbol{u}_h^{\varepsilon,n}-\boldsymbol{u}_h^{\varepsilon,n-1}\|^2+2\nu_0\|\boldsymbol{d}(\boldsymbol{u}_h^{\varepsilon,n})\|_{0,r}^r+\frac{1}{\varepsilon}\|\mathrm{div}\boldsymbol{u}_h^{\varepsilon,n}\|^2\\&+\frac{\alpha(\epsilon)}{2}\|\nabla \boldsymbol{u}_h^{\varepsilon,n}\|^2\le\frac{1}{2}\|\boldsymbol{f}(t^n)\|^2+\frac{1}{2}\|\boldsymbol{u}_h^{\varepsilon,n}\|^2+\frac{\alpha(\epsilon)}{4}\|S_H^n\|^2+\frac{\alpha(\epsilon)}{4}\|\nabla \boldsymbol{u}_h^{\varepsilon,n}\|^2.\end{aligned} \tag{4.6}$$

Noting that by choosing $\phi_H = S_H^n$ in $(3.16)_2$, using the Cauchy-Schwarz inequality and Young's inequality, we have

$$\|S_H^n\|^2=(\nabla \boldsymbol{u}_h^{\varepsilon,n-1},S_H^n)\le\|\nabla \boldsymbol{u}_h^{\varepsilon,n-1}\|\|S_H^n\|\le\frac{1}{2}\|\nabla \boldsymbol{u}_h^{\varepsilon,n-1}\|^2+\frac{1}{2}\|S_H^n\|^2.$$

Therefore, one obtains

$$\|S_H^n\|^2\le\|\nabla \boldsymbol{u}_h^{\varepsilon,n-1}\|^2. \tag{4.7}$$

We then arrive at the following result by inserting (4.7) into the inequality (4.6):

$$\begin{aligned}&\|\boldsymbol{u}_h^{\varepsilon,n}\|^2-\|\boldsymbol{u}_h^{\varepsilon,n-1}\|^2+\|\boldsymbol{u}_h^{\varepsilon,n}-\boldsymbol{u}_h^{\varepsilon,n-1}\|^2+\frac{4\nu_0\tau}{\rho}\|\boldsymbol{d}(\boldsymbol{u}_h^{\varepsilon,n})\|_{0,r}^r+\frac{2\tau}{\rho\varepsilon}\|\mathrm{div}\boldsymbol{u}_h^{\varepsilon,n}\|^2\\&+\frac{\alpha(\epsilon)\tau}{2\rho}(\|\nabla \boldsymbol{u}_h^{\varepsilon,n}\|^2-\|\nabla \boldsymbol{u}_h^{\varepsilon,n-1}\|^2)\le\frac{\tau}{\rho}\|\boldsymbol{f}(t^n)\|^2+\frac{\tau}{\rho}\|\boldsymbol{u}_h^{\varepsilon,n}\|^2.\end{aligned} \tag{4.8}$$

Summing of (4.8) for $n$ from 1 to $m$, $m = 1, 2, \cdots, N$, we get

$$\begin{aligned}&\|\boldsymbol{u}_h^{\varepsilon,m}\|^2+\sum_{n=1}^m\|\boldsymbol{u}_h^{\varepsilon,n}-\boldsymbol{u}_h^{\varepsilon,n-1}\|^2+\frac{\alpha(\epsilon)\tau}{2\rho}\|\nabla \boldsymbol{u}_h^{\varepsilon,m}\|^2+\frac{4\nu_0\tau}{\rho}\sum_{n=1}^m\|\boldsymbol{d}(\boldsymbol{u}_h^{\varepsilon,n})\|_{0,r}^r\\&+\frac{2\tau}{\rho\varepsilon}\sum_{n=1}^m\|\mathrm{div}\boldsymbol{u}_h^{\varepsilon,n}\|^2\le\|\boldsymbol{u}_h^{\varepsilon,0}\|^2+\frac{\alpha(\epsilon)\tau}{2\rho}\|\nabla \boldsymbol{u}_h^{\varepsilon,0}\|^2+\frac{\tau}{\rho}\sum_{n=1}^m\|\boldsymbol{f}(t^n)\|^2+\frac{\tau}{\rho}\sum_{n=1}^m\|\boldsymbol{u}_h^{\varepsilon,n}\|^2.\end{aligned}$$

Taking the maximum of the inequality above over $1 \le m \le N$, by virtue of the discrete Gronwall lemma and dropping a non-negative term, we obtain the desired bound (4.1).

Next, choosing $q_h = p_h^{\varepsilon,n}$ in $(3.16)_3$, combined with the Cauchy-Schwarz inequality and Young's inequality, leads to

$$\varepsilon\|p_h^{\varepsilon,n}\|^2=-(\mathrm{div}\boldsymbol{u}_h^{\varepsilon,n},p_h^{\varepsilon,n})\le\frac{1}{2\varepsilon}\|\mathrm{div}\boldsymbol{u}_h^{\varepsilon,n}\|^2+\frac{\varepsilon}{2}\|p_h^{\varepsilon,n}\|^2.$$

Therefore, we find that

$$\varepsilon\|p_h^{\varepsilon,n}\|^2\le\frac{1}{\varepsilon}\|\mathrm{div}\boldsymbol{u}_h^{\varepsilon,n}\|^2. \tag{4.9}$$

Summing (4.9) through $n$ from 1 to $N$, a direct consequence of (4.2) follows (4.1). This completes the proof.

**Theorem 4.2.** Assume that (**A1**) and (**A2**) hold. Let $(\boldsymbol{u}^\varepsilon, p^\varepsilon)$ be the solution of (2.9) and let $(\boldsymbol{u}_h^{\varepsilon,n}, p_h^{\varepsilon,n})$ be the solution of (3.16). Then, there is a generic constant $C > 0$, which is independent of $h$ and $\varepsilon$, such that

$$\begin{aligned}
&\max_{1\le m\le N} \|\boldsymbol{u}^\varepsilon(t^m) - \boldsymbol{u}_h^{\varepsilon,m}\|^2 + \frac{\alpha(\epsilon)\tau}{2\rho}\sum_{n=1}^{N}\|\nabla(\boldsymbol{u}^\varepsilon(t^n) - \boldsymbol{u}_h^{\varepsilon,n})\|^2 \\
&\quad + \frac{\nu_0\tau}{\rho}\sum_{n=1}^{N}\|\boldsymbol{u}^\varepsilon(t^n) - \boldsymbol{u}_h^{\varepsilon,n}\|_{1,r}^2 + \frac{\tau}{\rho\varepsilon}\sum_{n=1}^{N}\|\mathrm{div}(\boldsymbol{u}^\varepsilon(t^n) - \boldsymbol{u}_h^{\varepsilon,n})\|^2 \\
&\le C(\tau^2 + h^{2(k+1)} + h^{2k(r-1)} + h^{2k} + \alpha(\epsilon)h^{2k} + \alpha(\epsilon)H^{2k}),
\end{aligned} \tag{4.10}$$

and

$$\frac{\varepsilon\tau}{2\rho}\sum_{n=1}^{N}\|p^\varepsilon(t^n) - p_h^{\varepsilon,n}\|^2 \le C(\tau^2 + \varepsilon h^{2k} + h^{2k(r-1)} + h^{2k} + \alpha(\epsilon)h^{2k} + \alpha(\epsilon)H^{2k}). \tag{4.11}$$

**Proof.** Assume $\boldsymbol{e}^n = \boldsymbol{u}^\varepsilon(t^n) - \boldsymbol{u}_h^{\varepsilon,n}$. Subtracting (3.17) from (2.10) at $t = t^n$ with $\boldsymbol{v} = \boldsymbol{v}_h$, we obtain the following error equation:

$$\begin{aligned}
&\rho(\frac{\boldsymbol{e}^n - \boldsymbol{e}^{n-1}}{\tau}, \boldsymbol{v}_h) + \rho\{\widetilde{b}(\boldsymbol{u}^\varepsilon(t^n), \boldsymbol{u}^\varepsilon(t^n), \boldsymbol{v}_h) - \widetilde{b}(\boldsymbol{u}_h^{\varepsilon,n}, \boldsymbol{u}_h^{\varepsilon,n}, \boldsymbol{v}_h)\} + \frac{\alpha(\epsilon)}{2}(\nabla\boldsymbol{e}^n, \nabla\boldsymbol{v}_h) \\
&\quad + 2\nu_0\langle\mathcal{A}(\boldsymbol{u}^\varepsilon(t^n)) - \mathcal{A}(\boldsymbol{u}_h^{\varepsilon,n}), \boldsymbol{v}_h\rangle + \frac{1}{\varepsilon}(\mathrm{div}\boldsymbol{e}^n, \mathrm{div}\boldsymbol{v}_h) \\
&\quad + \frac{\alpha(\epsilon)}{2}(\nabla\boldsymbol{u}^\varepsilon(t^n) - P_H\nabla\boldsymbol{u}_h^{\varepsilon,n-1}, \nabla\boldsymbol{v}_h) = \rho(\boldsymbol{R}^n(\boldsymbol{u}^\varepsilon), \boldsymbol{v}_h),
\end{aligned} \tag{4.12}$$

where we can formulate the truncation error term as the integral residual of the Taylor series as follows:

$$\boldsymbol{R}^n(\boldsymbol{u}^\varepsilon) = \frac{\boldsymbol{u}^\varepsilon(t^n) - \boldsymbol{u}^\varepsilon(t^{n-1})}{\tau} - \frac{\partial}{\partial t}\boldsymbol{u}^\varepsilon(t^n) = \frac{1}{\tau}\int_{t^{n-1}}^{t^n}(t^n - t)\frac{\partial^2\boldsymbol{u}^\varepsilon}{\partial t^2}dt. \tag{4.13}$$

We decompose the velocity error in the usual way

$$\boldsymbol{e}^n = (\boldsymbol{u}^\varepsilon(t^n) - \Pi_h\boldsymbol{u}^\varepsilon(t^n)) + (\Pi_h\boldsymbol{u}^\varepsilon(t^n) - \boldsymbol{u}_h^{\varepsilon,n}) := \boldsymbol{\eta}^n + \boldsymbol{\xi}_h^n, \tag{4.14}$$

where $\Pi_h\boldsymbol{u}^\varepsilon$ denotes the finite element interpolation of $\boldsymbol{u}^\varepsilon$ in $\boldsymbol{X}_h$. Applying the error decomposition and taking $\boldsymbol{v}_h = \boldsymbol{\xi}_h^n$, by adding and subtracting $\mathcal{A}(\Pi_h\boldsymbol{u}^\varepsilon(t^n))$, we get

$$\begin{aligned}
&\frac{\rho}{2\tau}(\|\boldsymbol{\xi}_h^n\|^2 - \|\boldsymbol{\xi}_h^{n-1}\|^2) + \frac{\rho}{2\tau}\|\boldsymbol{\xi}_h^n - \boldsymbol{\xi}_h^{n-1}\|^2 + \frac{\alpha(\epsilon)}{2}\|\nabla\boldsymbol{\xi}_h^n\|^2 \\
&\quad + \frac{1}{\varepsilon}\|\mathrm{div}\boldsymbol{\xi}_h^n\|^2 + 2\nu_0\langle\mathcal{A}(\Pi_h\boldsymbol{u}^\varepsilon(t^n)) - \mathcal{A}(\boldsymbol{u}_h^{\varepsilon,n}), \boldsymbol{\xi}_h^n\rangle \\
&= -\rho(\frac{\boldsymbol{\eta}^n - \boldsymbol{\eta}^{n-1}}{\tau}, \boldsymbol{\xi}_h^n) - \rho\{\widetilde{b}(\boldsymbol{u}^\varepsilon(t^n), \boldsymbol{u}^\varepsilon(t^n), \boldsymbol{\xi}_h^n) - \widetilde{b}(\boldsymbol{u}_h^{\varepsilon,n}, \boldsymbol{u}_h^{\varepsilon,n}, \boldsymbol{\xi}_h^n)\} \\
&\quad - \frac{\alpha(\epsilon)}{2}(\nabla\boldsymbol{\eta}^n, \nabla\boldsymbol{\xi}_h^n) - 2\nu_0\langle\mathcal{A}(\boldsymbol{u}^\varepsilon(t^n)) - \mathcal{A}(\Pi_h\boldsymbol{u}^\varepsilon(t^n)), \boldsymbol{\xi}_h^n\rangle \\
&\quad - \frac{1}{\varepsilon}(\mathrm{div}\boldsymbol{\eta}^n, \mathrm{div}\boldsymbol{\xi}_h^n) - \frac{\alpha(\epsilon)}{2}(\nabla\boldsymbol{u}^\varepsilon(t^n) - P_H\nabla\boldsymbol{u}_h^{\varepsilon,n-1}, \nabla\boldsymbol{\xi}_h^n) + \rho(\boldsymbol{R}^n(\boldsymbol{u}^\varepsilon), \boldsymbol{\xi}_h^n).
\end{aligned} \tag{4.15}$$

The application of Lemma 2.1 and (**A2**) yields

$$\begin{aligned} 2\nu_0\langle \mathcal{A}(\Pi_h \boldsymbol{u}^\varepsilon(t^n)) - \mathcal{A}(\boldsymbol{u}_h^{\varepsilon,n}), \boldsymbol{\xi}_h^n\rangle &\geq 2\nu_0\eta\|\boldsymbol{\xi}_h^n\|_{1,r}^2(\|\Pi_h \boldsymbol{u}^\varepsilon(t^n)\|_{1,r} + \|\boldsymbol{u}_h^{\varepsilon,n}\|_{1,r})^{r-2} \\ &\geq \lambda_0\|\boldsymbol{\xi}_h^n\|_{1,r}^2, \end{aligned} \tag{4.16}$$

where we use the fact that $\|\Pi_h \boldsymbol{u}^\varepsilon(t^n)\|_{1,r} \leq C\|\boldsymbol{u}^\varepsilon(t^n)\|_{1,r}$ and set $\lambda_0 = 2\nu_0\eta(CK + K)^{r-2}$. Moreover, by virtue of Lemma 2.1, (3.8), and Young's inequality, it turns out that

$$\begin{aligned} -2\nu_0\langle \mathcal{A}(\boldsymbol{u}^\varepsilon(t^n)) - \mathcal{A}(\Pi_h \boldsymbol{u}^\varepsilon(t^n)), \boldsymbol{\xi}_h^n\rangle &\leq 2\nu_0\|\mathcal{A}(\boldsymbol{u}^\varepsilon(t^n)) - \mathcal{A}(\Pi_h \boldsymbol{u}^\varepsilon(t^n))\|_{-1,r'}\|\boldsymbol{\xi}_h^n\|_{1,r} \\ &\leq 2\nu_0\beta\|\boldsymbol{u}^\varepsilon(t^n) - \Pi_h \boldsymbol{u}^\varepsilon(t^n)\|_{1,r}^{r-1}\|\boldsymbol{\xi}_h^n\|_{1,r} \\ &\leq C(\|\boldsymbol{u}^\varepsilon(t^n)\|_{k+1,r})h^{2k(r-1)} + \frac{\lambda_0}{2}\|\boldsymbol{\xi}_h^n\|_{1,r}^2. \end{aligned} \tag{4.17}$$

After using the Cauchy-Schwarz inequality, the fundamental theorem of calculus, Poincaré-Friedrichs inequality, Young's inequality, and (3.8), we get

$$\begin{aligned} -\rho(\frac{\boldsymbol{\eta}^n - \boldsymbol{\eta}^{n-1}}{\tau}, \boldsymbol{\xi}_h^n) &\leq c\rho\|\frac{\boldsymbol{\eta}^n - \boldsymbol{\eta}^{n-1}}{\tau}\|\|\nabla\boldsymbol{\xi}_h^n\| \\ &\leq \frac{C}{\tau}\int_{t^{n-1}}^{t^n}\|\frac{\partial\boldsymbol{\eta}(t)}{\partial t}\|^2 dt + \frac{\alpha(\epsilon)}{12}\|\nabla\boldsymbol{\xi}_h^n\|^2 \\ &\leq \frac{Ch^{2(k+1)}}{\tau}\int_{t^{n-1}}^{t^n}\|\frac{\partial\boldsymbol{u}^\varepsilon}{\partial t}\|_{k+1,2}^2 dt + \frac{\alpha(\epsilon)}{24}\|\nabla\boldsymbol{\xi}_h^n\|^2. \end{aligned} \tag{4.18}$$

By adding and subtracting terms for the convective terms, and applying the properties (2.5), we rearrange the nonlinear terms as follows:

$$\begin{aligned} &-\rho\{\widetilde{b}(\boldsymbol{u}^\varepsilon(t^n), \boldsymbol{u}^\varepsilon(t^n), \boldsymbol{\xi}_h^n) - \widetilde{b}(\boldsymbol{u}_h^{\varepsilon,n}, \boldsymbol{u}_h^{\varepsilon,n}, \boldsymbol{\xi}_h^n)\} \\ &= -\rho\{\widetilde{b}(\boldsymbol{u}^\varepsilon(t^n), \boldsymbol{u}^\varepsilon(t^n), \boldsymbol{\xi}_h^n) - \widetilde{b}(\Pi_h \boldsymbol{u}^\varepsilon(t^n), \Pi_h \boldsymbol{u}^\varepsilon(t^n), \boldsymbol{\xi}_h^n) \\ &\quad + \widetilde{b}(\Pi_h \boldsymbol{u}^\varepsilon(t^n), \Pi_h \boldsymbol{u}^\varepsilon(t^n), \boldsymbol{\xi}_h^n) - \widetilde{b}(\boldsymbol{u}_h^{\varepsilon,n}, \boldsymbol{u}_h^{\varepsilon,n}, \boldsymbol{\xi}_h^n)\} \\ &= -\rho\widetilde{b}(\boldsymbol{u}^\varepsilon(t^n), \boldsymbol{\eta}^n, \boldsymbol{\xi}_h^n) - \rho\widetilde{b}(\boldsymbol{\eta}^n, \Pi_h \boldsymbol{u}^\varepsilon(t^n), \boldsymbol{\xi}_h^n) - \rho\widetilde{b}(\boldsymbol{\xi}_h^n, \boldsymbol{u}_h^{\varepsilon,n}, \boldsymbol{\xi}_h^n). \end{aligned} \tag{4.19}$$

We proceed to bound the convective terms by making use of the properties of $b$ and Young's inequality, which leads to

$$\begin{aligned} -\rho\widetilde{b}(\boldsymbol{u}^\varepsilon(t^n), \boldsymbol{\eta}^n, \boldsymbol{\xi}_h^n) &\leq \rho c\|\nabla\boldsymbol{u}^\varepsilon(t^n)\|\|\nabla\boldsymbol{\eta}^n\|\|\nabla\boldsymbol{\xi}_h^n\| \\ &\leq C\|\nabla\boldsymbol{u}^\varepsilon(t^n)\|^2\|\nabla\boldsymbol{\eta}^n\|^2 + \frac{\alpha(\epsilon)}{8}\|\nabla\boldsymbol{\xi}_h^n\|^2 \\ &\leq C(\|\boldsymbol{u}^\varepsilon(t^n)\|_{1,2}, \|\boldsymbol{u}^\varepsilon(t^n)\|_{k+1,2})h^{2k} + \frac{\alpha(\epsilon)}{24}\|\nabla\boldsymbol{\xi}_h^n\|^2, \end{aligned} \tag{4.20}$$

and

$$\begin{aligned} -\rho\widetilde{b}(\boldsymbol{\eta}^n, \Pi_h \boldsymbol{u}^\varepsilon(t^n), \boldsymbol{\xi}_h^n) &\leq \rho c\|\Pi_h \boldsymbol{u}^\varepsilon(t^n)\|_{1,2}\|\nabla\boldsymbol{\eta}^n\|\|\nabla\boldsymbol{\xi}_h^n\| \\ &\leq C\|\boldsymbol{u}^\varepsilon(t^n)\|_{1,2}^2\|\nabla\boldsymbol{\eta}^n\|^2 + \frac{\alpha(\epsilon)}{12}\|\nabla\boldsymbol{\xi}_h^n\|^2 \end{aligned}$$

$$\leq C(\|\boldsymbol{u}^{\varepsilon}(t^n)\|_{1,2}, \|\boldsymbol{u}^{\varepsilon}(t^n)\|_{k+1,2})h^{2k} + \frac{\alpha(\epsilon)}{24}\|\nabla\boldsymbol{\xi}_h^n\|^2, \tag{4.21}$$

and

$$\begin{aligned} -\rho\widetilde{b}(\boldsymbol{\xi}_h^n, \boldsymbol{u}_h^{\varepsilon,n}, \boldsymbol{\xi}_h^n) &\leq \rho c\|\nabla\boldsymbol{\xi}_h^n\|\|\boldsymbol{u}_h^{\varepsilon,n}\|_{2,2}\|\boldsymbol{\xi}_h^n\| \\ &\leq C\|\boldsymbol{u}_h^{\varepsilon,n}\|_{2,2}^2\|\boldsymbol{\xi}_h^n\|^2 + \frac{\alpha(\epsilon)}{24}\|\nabla\boldsymbol{\xi}_h^n\|^2. \end{aligned} \tag{4.22}$$

Thanks again to the Cauchy-Schwarz inequality, Young's inequality, and (3.8), we arrive at

$$-\frac{\alpha(\epsilon)}{2}(\nabla\boldsymbol{\eta}^n, \nabla\boldsymbol{\xi}_h^n) \leq \alpha(\epsilon)\|\nabla\boldsymbol{\eta}^n\|\|\nabla\boldsymbol{\xi}_h^n\| \leq C(\|\boldsymbol{u}^{\varepsilon}(t^n)\|_{k+1,2})h^{2k} + \frac{\alpha(\epsilon)}{24}\|\nabla\boldsymbol{\xi}_h^n\|^2, \tag{4.23}$$

and

$$-\frac{1}{\varepsilon}(\mathrm{div}\boldsymbol{\eta}^n, \mathrm{div}\boldsymbol{\xi}_h^n) \leq \frac{1}{\varepsilon}\|\nabla\boldsymbol{\eta}^n\|\|\mathrm{div}\boldsymbol{\xi}_h^n\| \leq C(\|\boldsymbol{u}^{\varepsilon}(t^n)\|_{k+1,2})h^{2k} + \frac{1}{2\varepsilon}\|\mathrm{div}\boldsymbol{\xi}_h^n\|^2, \tag{4.24}$$

where we use the div-grad relation $\|\mathrm{div}\boldsymbol{v}\| \leq \|\nabla\boldsymbol{v}\|$ for all $\boldsymbol{v} \in \boldsymbol{X}$. Next, we make an attempt to bound the coarse mesh projection term. By adding and subtracting $P_H\nabla\boldsymbol{u}^{\varepsilon}(t^{n-1})$ and $\nabla\boldsymbol{u}^{\varepsilon}(t^{n-1})$ to and from the coarse mesh projection term, making use of the error decomposition, Cauchy-Schwarz inequality, Young's inequality, inverse estimation, and (3.12)–(3.14) and (3.8), one obtains

$$\begin{aligned} &-\frac{\alpha(\epsilon)}{2}(\nabla\boldsymbol{u}^{\varepsilon}(t^n) - P_H\nabla\boldsymbol{u}_h^{\varepsilon,n-1}, \nabla\boldsymbol{\xi}_h^n) \\ &= -\frac{\alpha(\epsilon)}{2}(P_H\nabla\boldsymbol{e}^{n-1} + (\boldsymbol{I} - P_H)\nabla\boldsymbol{u}^{\varepsilon}(t^{n-1}) + (\nabla\boldsymbol{u}^{\varepsilon}(t^n) - \nabla\boldsymbol{u}^{\varepsilon}(t^{n-1})), \nabla\boldsymbol{\xi}_h^n) \\ &\leq C\alpha(\epsilon)(\|P_H\nabla\boldsymbol{\eta}^{n-1}\|^2 + \|P_H\nabla\boldsymbol{\xi}_h^{n-1}\|^2) + C\alpha(\epsilon)\|(\boldsymbol{I} - P_H)\nabla\boldsymbol{u}^{\varepsilon}(t^{n-1})\|^2 \\ &\quad + C\alpha(\epsilon)\|\nabla\boldsymbol{u}^{\varepsilon}(t^n) - \nabla\boldsymbol{u}^{\varepsilon}(t^{n-1})\|^2 + \frac{\alpha(\epsilon)}{24}\|\nabla\boldsymbol{\xi}_h^n\|^2 \\ &\leq C(\|\boldsymbol{u}^{\varepsilon}(t^{n-1})\|_{k+1,2})(\alpha(\epsilon)h^{2k} + \alpha(\epsilon)H^{2k}) + C\tau\|\nabla(\frac{\partial\boldsymbol{u}^{\varepsilon}}{\partial t})\|^2 \\ &\quad + C\alpha(\epsilon)h^{-2}\|\boldsymbol{\xi}_h^{n-1}\|^2 + \frac{\alpha(\epsilon)}{24}\|\nabla\boldsymbol{\xi}_h^n\|^2, \end{aligned} \tag{4.25}$$

where we use the fact that $\|P_H\boldsymbol{v}\| \leq \|\boldsymbol{v}\|$. Finally, we bound the local truncation error term as follows. Using the Cauchy-Schwarz inequality, Young's inequality, and Hölder's inequality, we obtain

$$\begin{aligned} \rho(\boldsymbol{R}^n(\boldsymbol{u}^{\varepsilon}), \boldsymbol{\xi}_h^n) &= (\frac{\rho}{\tau}\int_{t^{n-1}}^{t^n}(t^n - t)\frac{\partial^2\boldsymbol{u}^{\varepsilon}}{\partial t^2}dt, \boldsymbol{\xi}_h^n) \\ &\leq \|\frac{\rho}{\tau}\int_{t^{n-1}}^{t^n}(t^n - t)\frac{\partial^2\boldsymbol{u}^{\varepsilon}}{\partial t^2}dt\|\|\boldsymbol{\xi}_h^n\| \\ &\leq \frac{\rho\tau^2}{6}\int_{t^{n-1}}^{t^n}\|\frac{\partial^2\boldsymbol{u}^{\varepsilon}}{\partial t^2}\|^2dt + \frac{\rho}{2\tau}\|\boldsymbol{\xi}_h^n\|^2. \end{aligned} \tag{4.26}$$

Collecting all estimates (4.16)–(4.26) and rearranging the terms in (4.15), we get

$$\|\boldsymbol{\xi}_h^n\|^2 - \|\boldsymbol{\xi}_h^{n-1}\|^2 + \|\boldsymbol{\xi}_h^n - \boldsymbol{\xi}_h^{n-1}\|^2 + \frac{\alpha(\epsilon)\tau}{2\rho}\|\nabla\boldsymbol{\xi}_h^n\|^2 + \frac{\lambda_0\tau}{\rho}\|\boldsymbol{\xi}_h^n\|_{1,r}^2 + \frac{\tau}{\rho\varepsilon}\|\mathrm{div}\boldsymbol{\xi}_h^n\|^2$$

$$\leq Ch^{2(k+1)} + C\tau(h^{2k(r-1)} + h^{2k} + \alpha(\epsilon)h^{2k} + \alpha(\epsilon)H^{2k}) + C(\tau^2 + \tau^3)$$
$$+ C(\|\boldsymbol{\xi}_h^n\|^2 + \alpha(\epsilon)h^{-2}\|\boldsymbol{\xi}_h^{n-1}\|^2). \tag{4.27}$$

Noting the choice of $\alpha(\epsilon) = O(h^2)$, summing (4.27) from 1 to $m$, $m = 1, 2, \cdots, N$, applying the discrete Gronwall lemma, taking the maximum of the result from 1 to $N$, and dropping some non-negative terms leads to

$$\max_{1\leq m\leq N}\|\boldsymbol{\xi}_h^m\|^2 + \frac{\alpha(\epsilon)\tau}{2\rho}\sum_{n=1}^{N}\|\nabla\boldsymbol{\xi}_h^n\|^2 + \frac{\lambda_0\tau}{\rho}\sum_{n=1}^{N}\|\boldsymbol{\xi}_h^n\|_{1,r}^2 + \frac{\tau}{\rho\varepsilon}\sum_{n=1}^{N}\|\mathrm{div}\boldsymbol{\xi}_h^n\|^2$$
$$\leq C(\tau^2 + h^{2(k+1)} + h^{2k(r-1)} + h^{2k} + \alpha(\epsilon)h^{2k} + \alpha(\epsilon)H^{2k}). \tag{4.28}$$

Thus, the required bound (4.10) can be proved by applying the triangle inequality to the error decomposition.

For the pressure term, subtracting $(3.16)_3$ from $(2.9)_2$ with $q = q_h$ at $t = t^n$, yields

$$(\mathrm{div}(\boldsymbol{u}^\varepsilon(t^n) - \boldsymbol{u}_h^{\varepsilon,n}), q_h) + \varepsilon(p^\varepsilon(t^n) - p_h^{\varepsilon,n}, q_h) = 0. \tag{4.29}$$

Letting $p^\varepsilon(t^n) - p_h^{\varepsilon,n} = (p^\varepsilon(t^n) - \varrho_h p^\varepsilon(t^n)) + (\varrho_h p^\varepsilon(t^n) - p_h^{\varepsilon,n}) := \varphi^n + \psi_h^n$ and setting $q_h = \psi_h^n$ in (4.29), one obtains

$$\varepsilon\|\psi_h^n\|^2 = -(\mathrm{div}(\boldsymbol{u}^\varepsilon(t^n) - \boldsymbol{u}_h^{\varepsilon,n}), \psi_h^n) - \varepsilon(\varphi^n, \psi_h^n).$$

Using the Cauchy-Schwarz inequality, Young's inequality, and (3.10), we have

$$\varepsilon\|\psi_h^n\|^2 \leq |-(\mathrm{div}(\boldsymbol{u}^\varepsilon(t^n) - \boldsymbol{u}_h^{\varepsilon,n}), \psi_h^n)| + |-\varepsilon(\varphi^n, \psi_h^n)|$$
$$\leq \frac{1}{\varepsilon}\|\mathrm{div}(\boldsymbol{u}^\varepsilon(t^n) - \boldsymbol{u}_h^{\varepsilon,n})\|^2 + \frac{\varepsilon}{4}\|\psi_h^n\|^2 + \varepsilon\|\varphi^n\|^2 + \frac{\varepsilon}{4}\|\psi_h^n\|^2$$
$$\leq \frac{1}{\varepsilon}\|\mathrm{div}(\boldsymbol{u}^\varepsilon(t^n) - \boldsymbol{u}_h^{\varepsilon,n})\|^2 + \frac{\varepsilon}{2}\|\psi_h^n\|^2 + C(\|p^\varepsilon(t^n)\|_{k,2})\varepsilon h^{2k},$$

and hence

$$\frac{\varepsilon\tau}{2\rho}\|\psi_h^n\|^2 \leq \frac{\tau}{\rho\varepsilon}\|\mathrm{div}(\boldsymbol{u}^\varepsilon(t^n) - \boldsymbol{u}_h^{\varepsilon,n})\|^2 + C\varepsilon h^{2k}. \tag{4.30}$$

By summing (4.30) through $n$ from 1 to $N$, with the help of (4.10), and by applying the triangle inequality to the error decomposition, we prove (4.11).

**Corollary 4.1.** Assume that (**A1**) and (**A2**) hold. Let $(\boldsymbol{u}, p)$ be the solution of (2.8) and let $(\boldsymbol{u}_h^{\varepsilon,n}, p_h^{\varepsilon,n})$ be the solution of (3.16). Let the coarse mesh size $H = O(\sqrt{h})$ and the artificial viscosity parameter be $\alpha(\epsilon) = O(h^2)$. We then have

$$\max_{1\leq m\leq N}\|\boldsymbol{u}(t^m) - \boldsymbol{u}_h^{\varepsilon,m}\|^2 \leq C(\tau^2 + h^{2k(r-1)} + \varepsilon), \tag{4.31}$$

and

$$\frac{\varepsilon\tau}{2\rho}\sum_{n=1}^{N}\|p(t^n) - p_h^{\varepsilon,n}\|^2 \leq C(\tau^2 + h^{2k(r-1)} + \varepsilon h^{2k} + \varepsilon). \tag{4.32}$$

**Proof.** The combination of Theorems 3.1 and 4.2 immediately yields Corollary 4.1. We omit the proofs here.

*4.2. Numerical analysis of Algorithm 2.2*

**Theorem 4.3.** Assume that (**A1**) and (**A2**) hold. Then, the solution $(\boldsymbol{u}_h^{\varepsilon,n}, p_h^{\varepsilon,n})$ to the fully discrete formulation (3.18)–(3.20) is unconditionally stable. More precisely, we have

$$\begin{aligned}
&\max_{1\le m\le N}\{\|\boldsymbol{u}_h^{\varepsilon,m}\|^2+\frac{\alpha(\epsilon)\tau}{2\rho}\|\nabla\tilde{\boldsymbol{u}}_h^{\varepsilon,m}\|^2+\frac{\delta\tau^2}{\rho^2}\|\nabla\phi_h^{\varepsilon,m}\|^2\}+\sum_{n=1}^{N}\|\tilde{\boldsymbol{u}}_h^{\varepsilon,n}-\boldsymbol{u}_h^{\varepsilon,n-1}\|^2\\
&\quad+\frac{\delta-1}{2\delta}\sum_{n=1}^{N}\|\boldsymbol{u}_h^{\varepsilon,n}-\tilde{\boldsymbol{u}}_h^{\varepsilon,n}\|^2+\frac{4\nu_0\tau}{\rho}\sum_{n=1}^{N}\|\boldsymbol{d}(\tilde{\boldsymbol{u}}_h^{\varepsilon,n})\|_{0,r}^r+\frac{2\tau}{\rho\varepsilon}\sum_{n=1}^{N}\|\mathrm{div}\tilde{\boldsymbol{u}}_h^{\varepsilon,n}\|^2\\
&\le C(\|\boldsymbol{u}_h^{\varepsilon,0}\|^2+\|\nabla\boldsymbol{u}_h^{\varepsilon,0}\|^2+\|\nabla\phi_h^{\varepsilon,0}\|^2+\sum_{n=1}^{N}\|\boldsymbol{f}(t^n)\|^2),
\end{aligned}\tag{4.33}$$

$$\frac{2\varepsilon\tau}{\rho}\sum_{n=1}^{N}\|p_h^{\varepsilon,n}\|^2\le C(\|\boldsymbol{u}_h^{\varepsilon,0}\|^2+\|\nabla\boldsymbol{u}_h^{\varepsilon,0}\|^2+\|\nabla\phi_h^{\varepsilon,0}\|^2+\sum_{n=1}^{N}\|\boldsymbol{f}(t^n)\|^2),\tag{4.34}$$

where $C>0$ is a generic constant.

**Proof.** We first set $\boldsymbol{v}_h=\tilde{\boldsymbol{u}}_h^{\varepsilon,n}$ and $q_h=\mathrm{div}\tilde{\boldsymbol{u}}_h^{\varepsilon,n}$ in (3.18), putting together the results and using the orthogonal property of $\widetilde{b}$ to get

$$\begin{aligned}
&\rho(\frac{\tilde{\boldsymbol{u}}_h^{\varepsilon,n}-\boldsymbol{u}_h^{\varepsilon,n-1}}{\tau},\tilde{\boldsymbol{u}}_h^{\varepsilon,n})+2\nu_0\|\boldsymbol{d}(\tilde{\boldsymbol{u}}_h^{\varepsilon,n})\|_{0,r}^r+\frac{1}{\varepsilon}\|\mathrm{div}\tilde{\boldsymbol{u}}_h^{\varepsilon,n}\|^2+(\nabla\phi_h^{\varepsilon,n-1},\tilde{\boldsymbol{u}}_h^{\varepsilon,n})\\
&\quad+\frac{\alpha(\epsilon)}{2}\|\nabla\tilde{\boldsymbol{u}}_h^{\varepsilon,n}\|^2+\frac{\alpha(\epsilon)}{2}(S_H^n,\nabla\tilde{\boldsymbol{u}}_h^{\varepsilon,n})=(\boldsymbol{f}(t^n),\tilde{\boldsymbol{u}}_h^{\varepsilon,n}).
\end{aligned}$$

Thanks to the algebraic identity (4.4), we have

$$\begin{aligned}
&\frac{\rho}{2\tau}(\|\tilde{\boldsymbol{u}}_h^{\varepsilon,n}\|^2-\|\boldsymbol{u}_h^{\varepsilon,n-1}\|^2)+\frac{\rho}{2\tau}\|\tilde{\boldsymbol{u}}_h^{\varepsilon,n}-\boldsymbol{u}_h^{\varepsilon,n-1}\|^2+2\nu_0\|\boldsymbol{d}(\tilde{\boldsymbol{u}}_h^{\varepsilon,n})\|_{0,r}^r+\frac{1}{\varepsilon}\|\mathrm{div}\tilde{\boldsymbol{u}}_h^{\varepsilon,n}\|^2\\
&\quad+(\nabla\phi_h^{\varepsilon,n-1},\tilde{\boldsymbol{u}}_h^{\varepsilon,n})+\frac{\alpha(\epsilon)}{2}\|\nabla\tilde{\boldsymbol{u}}_h^{\varepsilon,n}\|^2=(\boldsymbol{f}(t^n),\tilde{\boldsymbol{u}}_h^{\varepsilon,n})-\frac{\alpha(\epsilon)}{2}(S_H^n,\nabla\tilde{\boldsymbol{u}}_h^{\varepsilon,n}).
\end{aligned}\tag{4.35}$$

On the other hand, we derive from $(3.19)_2$ that

$$(\boldsymbol{u}_h^{\varepsilon,n},\nabla\phi_h)=0.\tag{4.36}$$

On the basis of (4.4) and (4.36), we set $\boldsymbol{v}_h=\frac{\delta-1}{\delta}\tilde{\boldsymbol{u}}_h^{\varepsilon,n}$ in $(3.19)_1$ and obtain

$$\frac{\rho(\delta-1)}{2\tau\delta}(\|\boldsymbol{u}_h^{\varepsilon,n}\|^2-\|\tilde{\boldsymbol{u}}_h^{\varepsilon,n}\|^2+\|\boldsymbol{u}_h^{\varepsilon,n}-\tilde{\boldsymbol{u}}_h^{\varepsilon,n}\|^2)=0.\tag{4.37}$$

Moreover, we can derive

$$\|\tilde{\boldsymbol{u}}_h^{\varepsilon,n}\|^2=\|\boldsymbol{u}_h^{\varepsilon,n}\|^2+\|\boldsymbol{u}_h^{\varepsilon,n}-\tilde{\boldsymbol{u}}_h^{\varepsilon,n}\|^2.\tag{4.38}$$

Taking $\boldsymbol{v}_h=-\frac{1}{\delta}(\boldsymbol{u}_h^{\varepsilon,n}+\tilde{\boldsymbol{u}}_h^{\varepsilon,n})$ in $(3.19)_1$ and by (4.36), we have

$$-(\nabla\phi_h^{\varepsilon,n}-\nabla\phi_h^{\varepsilon,n-1},\tilde{\boldsymbol{u}}_h^{\varepsilon,n})=-(\nabla\phi_h^{\varepsilon,n}-\nabla\phi_h^{\varepsilon,n-1},\boldsymbol{u}_h^{\varepsilon,n}+\tilde{\boldsymbol{u}}_h^{\varepsilon,n})$$

$$= \frac{\rho}{\delta\tau}(\boldsymbol{u}_h^{\varepsilon,n} - \tilde{\boldsymbol{u}}_h^{\varepsilon,n}, \boldsymbol{u}_h^{\varepsilon,n} + \tilde{\boldsymbol{u}}_h^{\varepsilon,n})$$
$$= \frac{\rho}{\delta\tau}(\|\boldsymbol{u}_h^{\varepsilon,n}\|^2 - \|\tilde{\boldsymbol{u}}_h^{\varepsilon,n}\|^2). \tag{4.39}$$

Setting $\boldsymbol{v}_h = -\frac{\tau}{\rho}(\nabla\phi_h^{\varepsilon,n} + \nabla\phi_h^{\varepsilon,n-1})$ in $(3.19)_1$ and using (4.36), we obtain

$$(\nabla\phi_h^{\varepsilon,n} + \nabla\phi_h^{\varepsilon,n-1}, \tilde{\boldsymbol{u}}_h^{\varepsilon,n}) = -(\nabla\phi_h^{\varepsilon,n} + \nabla\phi_h^{\varepsilon,n-1}, \boldsymbol{u}_h^{\varepsilon,n} - \tilde{\boldsymbol{u}}_h^{\varepsilon,n})$$
$$= \frac{\delta\tau}{\rho}(\nabla\phi_h^{\varepsilon,n} + \nabla\phi_h^{\varepsilon,n-1}, \nabla\phi_h^{\varepsilon,n} - \nabla\phi_h^{\varepsilon,n-1})$$
$$= \frac{\delta\tau}{\rho}(\|\nabla\phi_h^{\varepsilon,n}\|^2 - \|\nabla\phi_h^{\varepsilon,n-1}\|^2). \tag{4.40}$$

Hence, adding (4.39) to (4.40), we arrive at

$$(\nabla\phi_h^{\varepsilon,n-1}, \tilde{\boldsymbol{u}}_h^{\varepsilon,n}) = \frac{\rho}{2\delta\tau}(\|\boldsymbol{u}_h^{\varepsilon,n}\|^2 - \|\tilde{\boldsymbol{u}}_h^{\varepsilon,n}\|^2) + \frac{\delta\tau}{2\rho}(\|\nabla\phi_h^{\varepsilon,n}\|^2 - \|\nabla\phi_h^{\varepsilon,n-1}\|^2). \tag{4.41}$$

Similar to the derivation of (4.7), by setting $\phi_H = S_H^n$ in $(3.18)_2$, we have

$$\|S_H^n\|^2 \le \|\nabla\tilde{\boldsymbol{u}}_h^{\varepsilon,n-1}\|^2. \tag{4.42}$$

Therefore, the first term on the right-hand side of (4.35) can be estimated by the Cauchy-Schwarz inequality, Young's inequality, and the identity (4.38), given as

$$(\boldsymbol{f}(t^n), \tilde{\boldsymbol{u}}_h^{\varepsilon,n}) \le \|\boldsymbol{f}(t^n)\|\|\tilde{\boldsymbol{u}}_h^{\varepsilon,n}\| \le C\|\boldsymbol{f}(t^n)\|^2 + \frac{\rho(\delta-1)}{4\tau\delta}\|\tilde{\boldsymbol{u}}_h^{\varepsilon,n}\|^2$$
$$\le C\|\boldsymbol{f}(t^n)\|^2 + \frac{\rho(\delta-1)}{4\tau\delta}\|\boldsymbol{u}_h^{\varepsilon,n}\|^2 + \frac{\rho(\delta-1)}{4\tau\delta}\|\boldsymbol{u}_h^{\varepsilon,n} - \tilde{\boldsymbol{u}}_h^{\varepsilon,n}\|^2. \tag{4.43}$$

Similarly, by virtue of (4.42), we can derive

$$-\frac{\alpha(\epsilon)}{2}(S_H^n, \nabla\tilde{\boldsymbol{u}}_h^{\varepsilon,n}) \le \frac{\alpha(\epsilon)}{4}\|S_H^n\|^2 + \frac{\alpha(\epsilon)}{4}\|\nabla\tilde{\boldsymbol{u}}_h^{\varepsilon,n}\|^2$$
$$\le \frac{\alpha(\epsilon)}{4}\|\nabla\tilde{\boldsymbol{u}}_h^{\varepsilon,n-1}\|^2 + \frac{\alpha(\epsilon)}{4}\|\nabla\tilde{\boldsymbol{u}}_h^{\varepsilon,n}\|^2. \tag{4.44}$$

Collecting (4.37), (4.41), (4.43), and (4.44) into (4.35), we get

$$\frac{\rho}{2\tau}(\|\boldsymbol{u}_h^{\varepsilon,n}\|^2 - \|\boldsymbol{u}_h^{\varepsilon,n-1}\|^2) + \frac{\rho}{2\tau}\|\tilde{\boldsymbol{u}}_h^{\varepsilon,n} - \boldsymbol{u}_h^{\varepsilon,n-1}\|^2 + \frac{\rho(\delta-1)}{4\tau\delta}\|\boldsymbol{u}_h^{\varepsilon,n} - \tilde{\boldsymbol{u}}_h^{\varepsilon,n}\|^2$$
$$+ 2\nu_0\|\boldsymbol{d}(\tilde{\boldsymbol{u}}_h^{\varepsilon,n})\|_{0,r}^r + \frac{1}{\varepsilon}\|\mathrm{div}\tilde{\boldsymbol{u}}_h^{\varepsilon,n}\|^2 + \frac{\delta\tau}{2\rho}(\|\nabla\phi_h^{\varepsilon,n}\|^2 - \|\nabla\phi_h^{\varepsilon,n-1}\|^2)$$
$$+ \frac{\alpha(\epsilon)}{4}(\|\nabla\tilde{\boldsymbol{u}}_h^{\varepsilon,n}\|^2 - \|\nabla\tilde{\boldsymbol{u}}_h^{\varepsilon,n-1}\|^2) \le C\|\boldsymbol{f}(t^n)\|^2 + \frac{\rho(\delta-1)}{4\tau\delta}\|\boldsymbol{u}_h^{\varepsilon,n}\|^2. \tag{4.45}$$

Taking the summation of (4.45) for $n$ from 1 to $m$, making use of the discrete Gronwall lemma, and taking the maximum of the result from 1 to $N$, the proof of (4.33) is complete.

We now treat the pressure term in similar way to the proof of (4.9), the following inequality can be arrived at:

$$\frac{\varepsilon\tau}{\rho}\|\tilde{p}_h^{\varepsilon,n}\|^2 \le \frac{\tau}{\rho\varepsilon}\|\mathrm{div}\tilde{\boldsymbol{u}}_h^{\varepsilon,n}\|^2. \tag{4.46}$$

From (3.20), using the Poincaré-Friedrichs inequality (2.3), we can obtain

$$\begin{aligned}\frac{\varepsilon\tau}{\rho}\|p_h^{\varepsilon,n}\|^2 &\le \frac{\varepsilon\tau}{\rho}\|\tilde{p}_h^{\varepsilon,n}\|^2 + \frac{\varepsilon\tau}{\rho}\|\phi_h^{\varepsilon,n}\|^2 + \frac{\varepsilon\tau\delta}{\rho}\|\phi_h^{\varepsilon,n} - \phi_h^{\varepsilon,n-1}\|^2\\ &\le \frac{\tau}{\rho\varepsilon}\|\mathrm{div}\tilde{\boldsymbol{u}}_h^{\varepsilon,n}\|^2 + \frac{c(1+2\delta)\varepsilon\tau}{\rho}\max_{1\le m\le N}\|\nabla\phi_h^{\varepsilon,m}\|^2.\end{aligned}$$

Summing the inequality above from $n = 1$ to $n = N$, by means of (4.33) and (4.46), we can obtain (4.34).

**Theorem 4.4.** Let $(\boldsymbol{u}^\varepsilon, p^\varepsilon)$ be the solution of (2.9) and let $(\boldsymbol{u}_h^{\varepsilon,n}, p_h^{\varepsilon,n})$ be the solution of (3.18)–(3.20), respectively. Then a generic constant $C > 0$ independent of $h$ and $\varepsilon$ exists, such that

$$\begin{aligned}&\max_{1\le m\le N}\|\boldsymbol{u}^\varepsilon(t^m) - \boldsymbol{u}_h^{\varepsilon,m}\|^2 + \frac{\alpha(\epsilon)\tau}{2\rho}\sum_{n=1}^{N}\|\nabla(\boldsymbol{u}^\varepsilon(t^n) - \tilde{\boldsymbol{u}}_h^{\varepsilon,n})\|^2\\ &\quad + \frac{\tau}{\rho\varepsilon}\sum_{n=1}^{N}\|\mathrm{div}(\boldsymbol{u}^\varepsilon(t^n) - \tilde{\boldsymbol{u}}_h^{\varepsilon,n})\|^2 + \frac{\lambda_0\tau}{\rho}\sum_{n=1}^{N}\|\boldsymbol{u}^\varepsilon(t^n) - \tilde{\boldsymbol{u}}_h^{\varepsilon,n}\|_{1,r}^2\\ &\le C(\tau^2 + h^{2k(r-1)} + h^{2k} + h^{2(k+1)} + \alpha(\epsilon)h^{2k} + \alpha(\epsilon)H^{2k}),\end{aligned} \tag{4.47}$$

and

$$\frac{\varepsilon\tau}{2\rho}\sum_{n=1}^{N}\|p^\varepsilon(t^n) - p_h^{\varepsilon,n}\|^2 \le C(\varepsilon + \tau^2 + \varepsilon h^{2k} + h^{2k(r-1)} + h^{2k} + \alpha(\epsilon)h^{2k} + \alpha(\epsilon)H^{2k}). \tag{4.48}$$

**Proof.** To begin with, we rewrite (3.18) as

$$\begin{aligned}&\rho(\frac{\tilde{\boldsymbol{u}}_h^{\varepsilon,n} - \boldsymbol{u}_h^{\varepsilon,n-1}}{\tau}, \boldsymbol{v}_h) + \rho\widetilde{b}(\tilde{\boldsymbol{u}}_h^{\varepsilon,n}, \tilde{\boldsymbol{u}}_h^{\varepsilon,n}, \boldsymbol{v}_h) + 2\nu_0\langle\mathcal{A}(\tilde{\boldsymbol{u}}_h^{\varepsilon,n}), \boldsymbol{v}_h\rangle + \frac{1}{\varepsilon}(\mathrm{div}\tilde{\boldsymbol{u}}_h^{\varepsilon,n}, \mathrm{div}\boldsymbol{v}_h)\\ &\quad + \frac{\alpha(\epsilon)}{2}(\nabla\tilde{\boldsymbol{u}}_h^{\varepsilon,n}, \nabla\boldsymbol{v}_h) + \frac{\alpha(\epsilon)}{2}(P_H\nabla\tilde{\boldsymbol{u}}_h^{\varepsilon,n-1}, \nabla\boldsymbol{v}_h) + (\nabla\phi_h^{\varepsilon,n-1}, \boldsymbol{v}_h) = (\boldsymbol{f}(t^n), \boldsymbol{v}_h).\end{aligned} \tag{4.49}$$

Define the errors $\boldsymbol{e}^n = \boldsymbol{u}^\varepsilon(t^n) - \boldsymbol{u}_h^{\varepsilon,n}$ and $\tilde{\boldsymbol{e}}^n = \boldsymbol{u}^\varepsilon(t^n) - \tilde{\boldsymbol{u}}_h^{\varepsilon,n}$. Subtracting (4.49) from (3.17) at $t = t^n$ with $\boldsymbol{v} = \boldsymbol{v}_h$, in light of (4.12), we obtain the following error equation:

$$\begin{aligned}&\rho(\frac{\tilde{\boldsymbol{e}}^n - \boldsymbol{e}^{n-1}}{\tau}, \boldsymbol{v}_h) + \rho\{\widetilde{b}(\boldsymbol{u}^\varepsilon(t^n), \boldsymbol{u}^\varepsilon(t^n), \boldsymbol{v}_h) - \widetilde{b}(\tilde{\boldsymbol{u}}_h^{\varepsilon,n}, \tilde{\boldsymbol{u}}_h^{\varepsilon,n}, \boldsymbol{v}_h)\} + \frac{\alpha(\epsilon)}{2}(\nabla\tilde{\boldsymbol{e}}^n, \nabla\boldsymbol{v}_h)\\ &\quad + 2\nu_0\langle\mathcal{A}(\boldsymbol{u}^\varepsilon(t^n)) - \mathcal{A}(\tilde{\boldsymbol{u}}_h^{\varepsilon,n}), \boldsymbol{v}_h\rangle + \frac{1}{\varepsilon}(\mathrm{div}\tilde{\boldsymbol{e}}^n, \mathrm{div}\boldsymbol{v}_h) - (\nabla\phi_h^{\varepsilon,n-1}, \boldsymbol{v}_h)\\ &\quad + \frac{\alpha(\epsilon)}{2}(\nabla\boldsymbol{u}^\varepsilon(t^n) - P_H\nabla\tilde{\boldsymbol{u}}_h^{\varepsilon,n-1}, \nabla\boldsymbol{v}_h) = \rho(\boldsymbol{R}^n(\boldsymbol{u}^\varepsilon), \boldsymbol{v}_h),\end{aligned} \tag{4.50}$$

where

$$\boldsymbol{R}^n(\boldsymbol{u}^\varepsilon) = \frac{\boldsymbol{u}^\varepsilon(t^n) - \boldsymbol{u}^\varepsilon(t^{n-1})}{\tau} - \frac{\partial}{\partial t}\boldsymbol{u}^\varepsilon(t^n) = \frac{1}{\tau}\int_{t^{n-1}}^{t^n}(t^n - t)\frac{\partial^2\boldsymbol{u}^\varepsilon}{\partial t^2}dt. \tag{4.51}$$

On the other hand, we derive the following from the projection system (3.19):

$$\rho(\frac{\boldsymbol{e}^n - \tilde{\boldsymbol{e}}^n}{\tau}, \boldsymbol{v}_h) + \delta(\nabla(\phi_h^{\varepsilon,n} - \phi_h^{\varepsilon,n-1}), \boldsymbol{v}_h) = 0, \tag{4.52}$$

and

$$(\mathrm{div}\boldsymbol{e}^n, q_h) = 0. \tag{4.53}$$

Before we embark on the error analysis, we decompose the errors as follows:

$$\begin{aligned}
\boldsymbol{e}^n &= (\boldsymbol{u}^\varepsilon(t^n) - \Pi_h\boldsymbol{u}^\varepsilon(t^n)) + (\Pi_h\boldsymbol{u}^\varepsilon(t^n) - \boldsymbol{u}_h^{\varepsilon,n}) := \boldsymbol{\eta}^n + \boldsymbol{\xi}_h^n,\\
\tilde{\boldsymbol{e}}^n &= (\boldsymbol{u}^\varepsilon(t^n) - \Pi_h\boldsymbol{u}^\varepsilon(t^n)) + (\Pi_h\boldsymbol{u}^\varepsilon(t^n) - \tilde{\boldsymbol{u}}_h^{\varepsilon,n}) := \boldsymbol{\eta}^n + \tilde{\boldsymbol{\xi}}_h^n,\\
\tilde{w}^n &= (p^\varepsilon(t^n) - \varrho_h p^\varepsilon(t^n)) + (\varrho_h p^\varepsilon(t^n) - \tilde{p}_h^{\varepsilon,n}) := \varphi^n + \tilde{\psi}_h^n.
\end{aligned}$$

Now, we rewrite the Eqs (4.50) and (4.52) as

$$\begin{aligned}
&\rho(\frac{\tilde{\boldsymbol{\xi}}_h^n - \boldsymbol{\xi}_h^{n-1}}{\tau}, \boldsymbol{v}_h) + \frac{\alpha(\epsilon)}{2}(\nabla\tilde{\boldsymbol{\xi}}_h^n, \nabla\boldsymbol{v}_h) + \frac{1}{\varepsilon}(\mathrm{div}\tilde{\boldsymbol{\xi}}_h^n, \mathrm{div}\boldsymbol{v}_h)\\
&\quad + 2\mu_0\langle\mathcal{A}(\Pi_h\boldsymbol{u}^\varepsilon(t^n)) - \mathcal{A}(\tilde{\boldsymbol{u}}_h^{\varepsilon,n}), \boldsymbol{v}_h\rangle - (\nabla\phi_h^{\varepsilon,n-1}, \boldsymbol{v}_h)\\
&= -\rho(\frac{\boldsymbol{\eta}^n - \boldsymbol{\eta}^{n-1}}{\tau}, \boldsymbol{v}_h) - \rho\{\widetilde{b}(\boldsymbol{u}^\varepsilon(t^n), \boldsymbol{u}^\varepsilon(t^n), \boldsymbol{v}_h) - \widetilde{b}(\tilde{\boldsymbol{u}}_h^{\varepsilon,n}, \tilde{\boldsymbol{u}}_h^{\varepsilon,n}, \boldsymbol{v}_h)\}\\
&\quad - 2\mu_0\langle\mathcal{A}(\boldsymbol{u}^\varepsilon(t^n)) - \mathcal{A}(\Pi_h\boldsymbol{u}^\varepsilon(t^n)), \boldsymbol{v}_h\rangle - \frac{\alpha(\epsilon)}{2}(\nabla\boldsymbol{\eta}^n, \nabla\boldsymbol{v}_h) - \frac{1}{\varepsilon}(\mathrm{div}\boldsymbol{\eta}^n, \mathrm{div}\boldsymbol{v}_h)\\
&\quad - \frac{\alpha(\epsilon)}{2}(\nabla\boldsymbol{u}^\varepsilon(t^n) - P_H\nabla\tilde{\boldsymbol{u}}_h^{\varepsilon,n-1}, \nabla\boldsymbol{v}_h) + \rho(\boldsymbol{R}^n(\boldsymbol{u}^\varepsilon), \boldsymbol{v}_h),
\end{aligned} \tag{4.54}$$

and

$$\rho(\frac{\boldsymbol{\xi}_h^n - \tilde{\boldsymbol{\xi}}_h^n}{\tau}, \boldsymbol{v}_h) - \delta(\nabla(\phi_h^{\varepsilon,n} - \phi_h^{\varepsilon,n-1}), \boldsymbol{v}_h) = 0. \tag{4.55}$$

Notice that from (3.9) and (4.53), it follows that

$$(\boldsymbol{\xi}_h^n, \nabla\phi_h) = (\boldsymbol{e}^n, \nabla\phi_h) - (\boldsymbol{\eta}^n, \nabla\phi_h) = 0. \tag{4.56}$$

Let us take $\boldsymbol{v}_h = \frac{\delta-1}{\delta}\boldsymbol{\xi}_h^n$ in (4.55), in which case

$$\frac{\rho(\delta-1)}{2\tau\delta}(\|\boldsymbol{\xi}_h^n\|^2 - \|\tilde{\boldsymbol{\xi}}_h^n\|^2 + \|\boldsymbol{\xi}_h^n - \tilde{\boldsymbol{\xi}}_h^n\|^2) = 0. \tag{4.57}$$

Choosing $\boldsymbol{v}_h = \frac{1}{\delta}(\boldsymbol{\xi}_h^n + \tilde{\boldsymbol{\xi}}_h^n)$ in (4.55) yields

$$\frac{\rho}{\delta\tau}(\|\boldsymbol{\xi}_h^n\|^2 - \|\tilde{\boldsymbol{\xi}}_h^n\|^2) - (\nabla(\phi_h^{\varepsilon,n} - \phi_h^{\varepsilon,n-1}), \tilde{\boldsymbol{\xi}}_h^n) = 0. \tag{4.58}$$

From (4.55), we have

$$\tilde{\boldsymbol{\xi}}_h^n = \boldsymbol{\xi}_h^n - \frac{\delta\tau}{\rho}\nabla(\phi_h^{\varepsilon,n} - \phi_h^{\varepsilon,n-1}). \tag{4.59}$$

Therefore, we can obtain

$$(\nabla(\phi_h^{\varepsilon,n} + \phi_h^{\varepsilon,n-1}), \tilde{\boldsymbol{\xi}}_h^n) = -\frac{\delta\tau}{\rho}(\|\nabla\phi_h^{\varepsilon,n}\|^2 - \|\nabla\phi_h^{\varepsilon,n-1}\|^2). \tag{4.60}$$

Now we take $\boldsymbol{v}_h = \tilde{\boldsymbol{\xi}}_h^n$ in (4.54); combine it with (4.57), (4.58), and (4.60); and arrange the results. We derive

$$\begin{aligned}
&\frac{\rho}{2\tau}(\|\boldsymbol{\xi}_h^n\|^2 - \|\boldsymbol{\xi}_h^{n-1}\|^2) + \frac{\rho}{2\tau}\|\tilde{\boldsymbol{\xi}}_h^n - \boldsymbol{\xi}_h^{n-1}\|^2 + \frac{\rho(\delta-1)}{2\tau\delta}\|\boldsymbol{\xi}_h^n - \tilde{\boldsymbol{\xi}}_h^n\|^2 + \frac{\alpha(\epsilon)}{2}\|\nabla\tilde{\boldsymbol{\xi}}_h^n\|^2 \\
&\quad + \frac{1}{\varepsilon}\|\mathrm{div}\tilde{\boldsymbol{\xi}}_h^n\|^2 + \frac{\delta\tau}{2\rho}(\|\nabla\phi_h^{\varepsilon,n}\|^2 - \|\nabla\phi_h^{\varepsilon,n-1}\|^2) + 2\nu_0\langle\mathcal{A}(\Pi_h\boldsymbol{u}^\varepsilon(t^n)) - \mathcal{A}(\tilde{\boldsymbol{u}}_h^{\varepsilon,n}), \tilde{\boldsymbol{\xi}}_h^n\rangle \\
&= -\rho(\frac{\boldsymbol{\eta}^n - \boldsymbol{\eta}^{n-1}}{\tau}, \tilde{\boldsymbol{\xi}}_h^n) - \rho\{\widetilde{b}(\boldsymbol{u}^\varepsilon(t^n), \boldsymbol{u}^\varepsilon(t^n), \tilde{\boldsymbol{\xi}}_h^n) - \widetilde{b}(\tilde{\boldsymbol{u}}_h^{\varepsilon,n}, \tilde{\boldsymbol{u}}_h^{\varepsilon,n}, \tilde{\boldsymbol{\xi}}_h^n)\} \\
&\quad - 2\nu_0\langle\mathcal{A}(\boldsymbol{u}^\varepsilon(t^n)) - \mathcal{A}(\Pi_h\boldsymbol{u}^\varepsilon(t^n)), \tilde{\boldsymbol{\xi}}_h^n\rangle - \frac{\alpha(\epsilon)}{2}(\nabla\boldsymbol{\eta}^n, \nabla\tilde{\boldsymbol{\xi}}_h^n) - \frac{1}{\varepsilon}(\mathrm{div}\boldsymbol{\eta}^n, \mathrm{div}\tilde{\boldsymbol{\xi}}_h^n) \\
&\quad - \frac{\alpha(\epsilon)}{2}(\nabla\boldsymbol{u}^\varepsilon(t^n) - P_H\nabla\tilde{\boldsymbol{u}}_h^{\varepsilon,n-1}, \nabla\tilde{\boldsymbol{\xi}}_h^n) + \rho(\boldsymbol{R}^n(\boldsymbol{u}^\varepsilon), \tilde{\boldsymbol{\xi}}_h^n).
\end{aligned} \tag{4.61}$$

We proceed exactly as in the proofs of (4.16)–(4.18), (4.23), and (4.24), and thus

$$2\nu_0\langle\mathcal{A}(\Pi_h\boldsymbol{u}^\varepsilon(t^n)) - \mathcal{A}(\tilde{\boldsymbol{u}}_h^{\varepsilon,n}), \tilde{\boldsymbol{\xi}}_h^n\rangle \geq \lambda_0\|\tilde{\boldsymbol{\xi}}_h^n\|_{1,r}^2, \tag{4.62}$$

$$-2\nu_0\langle\mathcal{A}(\boldsymbol{u}^\varepsilon(t^n)) - \mathcal{A}(\Pi_h\boldsymbol{u}^\varepsilon(t^n)), \tilde{\boldsymbol{\xi}}_h^n\rangle \leq C(\|\boldsymbol{u}^\varepsilon(t^n)\|_{k+1,r})h^{2k(r-1)} + \frac{\lambda_0}{2}\|\tilde{\boldsymbol{\xi}}_h^n\|_{1,r}^2, \tag{4.63}$$

$$-\rho(\frac{\boldsymbol{\eta}^n - \boldsymbol{\eta}^{n-1}}{\tau}, \tilde{\boldsymbol{\xi}}_h^n) \leq \frac{Ch^{2(k+1)}}{\tau}\int_{t^{n-1}}^{t^n}\|\frac{\partial\boldsymbol{u}^\varepsilon}{\partial t}\|_{k+1,2}^2 dt + \frac{\alpha(\epsilon)}{24}\|\nabla\tilde{\boldsymbol{\xi}}_h^n\|^2, \tag{4.64}$$

$$-\frac{\alpha(\epsilon)}{2}(\nabla\boldsymbol{\eta}^n, \nabla\tilde{\boldsymbol{\xi}}_h^n) \leq C(\|\boldsymbol{u}^\varepsilon(t^n)\|_{k+1,2})h^{2k} + \frac{\alpha(\epsilon)}{24}\|\nabla\tilde{\boldsymbol{\xi}}_h^n\|^2, \tag{4.65}$$

$$-\frac{1}{\varepsilon}(\mathrm{div}\boldsymbol{\eta}^n, \mathrm{div}\tilde{\boldsymbol{\xi}}_h^n) \leq C(\|\boldsymbol{u}^\varepsilon(t^n)\|_{k+1,2})h^{2k} + \frac{1}{2\varepsilon}\|\mathrm{div}\tilde{\boldsymbol{\xi}}_h^n\|^2. \tag{4.66}$$

Note that from (4.57), one gets

$$\|\tilde{\boldsymbol{\xi}}_h^n\|^2 = \|\boldsymbol{\xi}_h^n\|^2 + \|\boldsymbol{\xi}_h^n - \tilde{\boldsymbol{\xi}}_h^n\|^2. \tag{4.67}$$

Then the convective terms can be estimated by the same techniques as in (4.19)–(4.21), and by using (4.67), we obtain

$$\begin{aligned}
&-\rho\{\widetilde{b}(\boldsymbol{u}^\varepsilon(t^n), \boldsymbol{u}^\varepsilon(t^n), \tilde{\boldsymbol{\xi}}_h^n) - \widetilde{b}(\tilde{\boldsymbol{u}}_h^{\varepsilon,n}, \tilde{\boldsymbol{u}}_h^{\varepsilon,n}, \tilde{\boldsymbol{\xi}}_h^n)\} \\
&\leq Ch^{2k} + \frac{\alpha(\epsilon)}{8}\|\nabla\tilde{\boldsymbol{\xi}}_h^n\|^2 + C\|\tilde{\boldsymbol{u}}_h^{\varepsilon,n}\|_{2,2}^2\|\tilde{\boldsymbol{\xi}}_h^n\|^2
\end{aligned}$$

$$= Ch^{2k} + \frac{\alpha(\epsilon)}{8}\|\nabla\tilde{\boldsymbol{\xi}}_h^n\|^2 + C\|\tilde{\boldsymbol{u}}_h^{\varepsilon,n}\|_{2,2}^2(\|\boldsymbol{\xi}_h^n\|^2 + \|\boldsymbol{\xi}_h^n - \tilde{\boldsymbol{\xi}}_h^n\|^2). \tag{4.68}$$

By similar computations as in (4.25), we have

$$\begin{aligned}
&-\frac{\alpha(\epsilon)}{2}(\nabla\boldsymbol{u}^{\varepsilon}(t^n) - P_H\nabla\tilde{\boldsymbol{u}}_h^{\varepsilon,n-1}, \nabla\tilde{\boldsymbol{\xi}}_h^n)\\
&\le C(\|\boldsymbol{u}^{\varepsilon}(t^{n-1})\|_{k+1,2})(\alpha(\epsilon)h^{2k} + \alpha(\epsilon)H^{2k}) + C\alpha(\epsilon)\tau^2\|\nabla(\frac{\partial\boldsymbol{u}^{\varepsilon}}{\partial t})\|^2\\
&\quad + C\alpha(\epsilon)h^{-2}\|\tilde{\boldsymbol{\xi}}_h^{n-1}\|^2 + \frac{\alpha(\epsilon)}{24}\|\nabla\tilde{\boldsymbol{\xi}}_h^n\|^2\\
&= C(\|\boldsymbol{u}^{\varepsilon}(t^{n-1})\|_{k+1,2})(\alpha(\epsilon)h^{2k} + \alpha(\epsilon)H^{2k}) + C\alpha(\epsilon)\tau^2\|\nabla(\frac{\partial\boldsymbol{u}^{\varepsilon}}{\partial t})\|^2\\
&\quad + C\alpha(\epsilon)h^{-2}(\|\boldsymbol{\xi}_h^{n-1}\|^2 + \|\boldsymbol{\xi}_h^{n-1} - \tilde{\boldsymbol{\xi}}_h^{n-1}\|^2) + \frac{\alpha(\epsilon)}{24}\|\nabla\tilde{\boldsymbol{\xi}}_h^n\|^2.
\end{aligned} \tag{4.69}$$

Applying the Cauchy-Schwarz inequality, Young's inequality, and Hölder inequality, we arrive at

$$\begin{aligned}
\rho(\boldsymbol{R}^n(\boldsymbol{u}^{\varepsilon}), \tilde{\boldsymbol{\xi}}_h^n) &\le |(\frac{\rho}{\tau}\int_{t^{n-1}}^{t^n}(t^n - t)\frac{\partial^2\boldsymbol{u}^{\varepsilon}}{\partial t^2}dt, \tilde{\boldsymbol{\xi}}_h^n)|\\
&\le \frac{\rho\delta\tau^2}{3(\delta-1)}\int_{t^{n-1}}^{t^n}\|\frac{\partial^2\boldsymbol{u}^{\varepsilon}}{\partial t^2}\|^2dt + \frac{\rho(\delta-1)}{4\tau\delta}\|\tilde{\boldsymbol{\xi}}_h^n\|^2\\
&= \frac{\rho\delta\tau^2}{3(\delta-1)}\int_{t^{n-1}}^{t^n}\|\frac{\partial^2\boldsymbol{u}^{\varepsilon}}{\partial t^2}\|^2dt + \frac{\rho(\delta-1)}{4\tau\delta}(\|\boldsymbol{\xi}_h^n\|^2 + \|\boldsymbol{\xi}_h^n - \tilde{\boldsymbol{\xi}}_h^n\|^2).
\end{aligned} \tag{4.70}$$

We can choose $\delta$ and $\epsilon$ such that $\mu_0 = \frac{\rho(\delta-1)}{4\tau\delta} - C\|\tilde{\boldsymbol{u}}_h^{\varepsilon,n}\|_{2,2}^2 - C\alpha(\epsilon)h^{-2} > 0$. By combining these inequalities (4.62)–(4.70) into (4.61), we obtain

$$\begin{aligned}
&\|\boldsymbol{\xi}_h^n\|^2 - \|\boldsymbol{\xi}_h^{n-1}\|^2 + \|\tilde{\boldsymbol{\xi}}_h^n - \boldsymbol{\xi}_h^{n-1}\|^2 + \frac{2\mu_0\tau}{\rho}(\|\boldsymbol{\xi}_h^n - \tilde{\boldsymbol{\xi}}_h^n\|^2 - \|\boldsymbol{\xi}_h^{n-1} - \tilde{\boldsymbol{\xi}}_h^{n-1}\|^2) + \frac{\alpha(\epsilon)\tau}{2\rho}\|\nabla\tilde{\boldsymbol{\xi}}_h^n\|^2\\
&\quad + \frac{\tau}{\rho\varepsilon}\|\mathrm{div}\tilde{\boldsymbol{\xi}}_h^n\|^2 + \frac{\lambda_0\tau}{\rho}\|\tilde{\boldsymbol{\xi}}_h^n\|_{1,r}^2 + \frac{\delta\tau^2}{\rho^2}(\|\nabla\phi_h^{\varepsilon,n}\|^2 - \|\nabla\phi_h^{\varepsilon,n-1}\|^2)\\
&\le C(\tau^2 + \tau^3) + Ch^{2(k+1)} + C\tau(h^{2k(r-1)} + h^{2k} + \alpha(\epsilon)h^{2k} + \alpha(\epsilon)H^{2k})\\
&\quad + C(\|\boldsymbol{\xi}_h^n\|^2 + \alpha(\epsilon)h^{-2}\|\boldsymbol{\xi}_h^{n-1}\|^2).
\end{aligned} \tag{4.71}$$

Summing (4.71) for $n = 1$ to $n = m$ and using Lemma 2.5 gives

$$\begin{aligned}
&\|\boldsymbol{\xi}_h^m\|^2 + \sum_{n=1}^{m}\|\tilde{\boldsymbol{\xi}}_h^n - \boldsymbol{\xi}_h^{n-1}\|^2 + \frac{2\mu_0\tau}{\rho}\|\boldsymbol{\xi}_h^m - \tilde{\boldsymbol{\xi}}_h^m\|^2 + \frac{\alpha(\epsilon)\tau}{2\rho}\sum_{n=1}^{m}\|\nabla\tilde{\boldsymbol{\xi}}_h^n\|^2\\
&\quad + \frac{\tau}{\rho\varepsilon}\sum_{n=1}^{m}\|\mathrm{div}\tilde{\boldsymbol{\xi}}_h^n\|^2 + \frac{\lambda_0\tau}{\rho}\sum_{n=1}^{m}\|\tilde{\boldsymbol{\xi}}_h^n\|_{1,r}^2 + \frac{\delta\tau^2}{\rho^2}\|\nabla\phi_h^{\varepsilon,m}\|^2\\
&\le C(\tau^2 + h^{2(k+1)} + h^{2k(r-1)} + h^{2k} + \alpha(\epsilon)h^{2k} + \alpha(\epsilon)H^{2k}).
\end{aligned}$$

Taking the maximum of the result from 1 to $N$, applying the triangle inequality to the error decomposition, and dropping some positive terms, one obtains the desired result (4.47).

Finally, subtracting $(3.18)_3$ from $(2.9)_2$ with $q = q_h$ at $t = t^n$, leads to

$$(\mathrm{div}(\boldsymbol{u}^{\varepsilon}(t^n) - \tilde{\boldsymbol{u}}_h^{\varepsilon,n}), q_h) + \varepsilon(p^{\varepsilon}(t^n) - \tilde{p}_h^{\varepsilon,n}, q_h) = 0. \tag{4.72}$$

We take $q_h = p^{\varepsilon}(t^n) - \tilde{p}_h^{\varepsilon,n}$ in (4.72), similar to the proof of (4.9), and obtain

$$\frac{\varepsilon\tau}{\rho}\|p^{\varepsilon}(t^n) - \tilde{p}_h^{\varepsilon,n}\|^2 \le \frac{\tau}{\rho\varepsilon}\|\mathrm{div}(\boldsymbol{u}^{\varepsilon}(t^n) - \tilde{\boldsymbol{u}}_h^{\varepsilon,n})\|^2. \tag{4.73}$$

Making use of (3.20), (4.73), and the Poincaré-Friedrichs inequality, we get

$$\begin{aligned}\frac{\varepsilon\tau}{\rho}\|p^{\varepsilon}(t^n) - p_h^{\varepsilon,n}\|^2 &\le \frac{\varepsilon\tau}{\rho}\|p^{\varepsilon}(t^n) - \tilde{p}_h^{\varepsilon,n}\|^2 + \frac{\varepsilon\tau}{\rho}\|\phi_h^{\varepsilon,n}\|^2 + \frac{\varepsilon\tau\delta}{\rho}\|\phi_h^{\varepsilon,n} - \phi_h^{\varepsilon,n-1}\|^2 \\ &\le \frac{\tau}{\rho\varepsilon}\|\mathrm{div}(\boldsymbol{u}^{\varepsilon}(t^n) - \tilde{\boldsymbol{u}}_h^{\varepsilon,n})\|^2 + \frac{\varepsilon c(1+2\delta)\tau}{\rho}\max_{1\le m\le N}\|\nabla\phi_h^{\varepsilon,m}\|^2. \end{aligned}\tag{4.74}$$

Summing up (4.74) from $n = 1$ to $n = N$, and using (4.33) and (4.47), we can obtain (4.48). The proof is finished.

**Corollary 4.2.** Assume that (**A1**) and (**A2**) hold. Let $(\boldsymbol{u}, p)$ be the solution of (2.8) and let $(\boldsymbol{u}_h^{\varepsilon,n}, p_h^{\varepsilon,n})$ be the solution of (3.18)–(3.20). Let the coarse mesh size be $H = O(\sqrt{h})$ and the artificial viscosity parameter be $\alpha(\epsilon) = O(h^2)$. We then have

$$\max_{1\le m\le N}\|\boldsymbol{u}(t^m) - \boldsymbol{u}_h^{\varepsilon,m}\|^2 \le C(\tau^2 + h^{2k(r-1)} + \varepsilon), \tag{4.75}$$

and

$$\frac{\varepsilon\tau}{2\rho}\sum_{n=1}^{N}\|p(t^n) - p_h^{\varepsilon,n}\|^2 \le C(\tau^2 + h^{2k(r-1)} + \varepsilon h^{2k} + \varepsilon). \tag{4.76}$$

**Proof.** We omit the proofs of (4.75) and (4.76), since the proofs are straightforward.

## 5. Numerical experiments

The objective of this section is to perform a comparison between the proposed schemes presented here, and we also elucidate certain properties of the non-Newtonian flow studied. Moreover, the artificial viscosity penalty projection finite element method is widely used in the study of aneurysmal disease. Several numerical tests are presented for validating the support of the derived theoretical results and to underline the efficiency of the schemes. First of all, the numerical iterations solve for the following power-law term that is of importance to us:

$$\langle\mathcal{A}(\boldsymbol{u}), \boldsymbol{v}\rangle = (|\boldsymbol{d}(\boldsymbol{u})|^{r-2}\boldsymbol{d}(\boldsymbol{u}), \boldsymbol{d}(\boldsymbol{v})), \tag{5.1}$$

which is solved iteratively by introducing the dependent variable

$$\boldsymbol{M}_j := \begin{cases} 1 & j = 1, \\ \gamma\boldsymbol{M}_{j-1} + (1-\gamma)|\boldsymbol{d}(\boldsymbol{u}_j)|^{r-2} & j > 1, \end{cases} \tag{5.2}$$

where $j \in \mathbb{N}$ is, of course, the iteration index. The value of $\gamma$ affects the convergence properties of the solution process. In the example, $\gamma$ is chosen to be 0.1, which seems to work for $1.2 \le r \le 2$ but becomes less stable for $1 < r < 1.2$. For $r < 1.2$, it seems to need a $\gamma$ that converges (slowly enough) to one. Note that $\gamma = 0$ seems to be unstable or at least oscillatory for all values of$r$.

*5.1. The convergence and validity of algorithms.*

In this first set of numerical simulations, we would like to test the convergence and validity of the algorithms obtained in previous sections. The performance of the proposed schemes are investigated with the penalty parameter $\varepsilon = 10^{-6}$ (which goes to zero), we choose the artificial viscosity parameter $\alpha(\epsilon) = 0.01h^2$ (which as tends to zero) and the coarse mesh size $H = \sqrt{h}$. We note that in each computation, the fine mesh is a square refinement of the coarse mesh.

As a first benchmark for the proposed methods, we use the standard benchmark of a lid-driven cavity flow problem for assessing the performance of the algorithms. The chosen computational domain is $\Omega = [0, 1]^2$, and we assume the exterior force to be unity. The density is set to $\rho = 1.06$ and the viscosity to $\eta_0 = 0.012$. The velocity and pressure will be approximated by $P_2 - P_1$ finite elements on a uniform mesh. Since we do not have the exact solution of the given problem, we compute the error using the difference of the solution obtained for $h = \frac{1}{M/2}$ and $h^* = \frac{1}{M^*/2}$, where $M + 1$ is the number of grid points of $[0, 1]$ and $M^* + 1 = 2(M + 1) - 1$.

We only address the accuracy of the spatial discretization with a small time increment $\tau = 10^{-3}$ (the accuracy of the temporal discretization is usually first-order, so we omit it here). The errors and convergence rates for the non-Newtonian cases with the power-law index $r = 1.5$ and $r = 1.8$ at the time $t = 0.1$ are reported in Tables 1 and 2, where $\boldsymbol{U}_h^n$ represents $\boldsymbol{u}_h^n$ or $\boldsymbol{u}_h^{\varepsilon,n}$, and $P_h^n$ stands for $p_h^n$ or $p_h^{\varepsilon,n}$ respectively. From Tables 1 and 2, we can see that the convergence order of Algorithms 3.2 and 3.3 are slightly higher than that of Algorithm 3.1. The numerical results show that the convergence orders of the errors for the velocity field $\boldsymbol{u}$ and the pressure $p$ are close to $O(h^{2(r-1)})$, which are consistent with the theory established in Section 4.

**Table 1.** Numerical errors and convergence orders for the velocity field $\boldsymbol{u}$ and the pressure $p$ in spatial direction with $\tau = 10^{-3}$ and $r = 1.5$.

| Method | $h$ | $\|\boldsymbol{u}(t^n) - \boldsymbol{U}_h^n\|$ | Rate | $\|p(t^n) - P_h^n\|$ | Rate |
|---|---|---|---|---|---|
| Algorithm 3.1 | 1/16 | 8.4562e-02 | - | 9.3865e-01 | - |
| | 1/32 | 1.5868e-02 | 0.98 | 1.7439e-01 | 0.99 |
| | 1/64 | 7.6231e-03 | 1.02 | 8.6327e-02 | 1.00 |
| | 1/128 | 3.9277e-03 | 0.99 | 4.2734e-02 | 1.01 |
| Algorithm 3.2 | 1/16 | 4.8749e-02 | - | 8.9783e-01 | - |
| | 1/32 | 8.4446e-03 | 1.06 | 1.6026e-01 | 1.03 |
| | 1/64 | 4.1387e-03 | 1.08 | 8.0938e-02 | 1.02 |
| | 1/128 | 2.0285e-03 | 1.10 | 4.0066e-02 | 1.03 |
| Algorithm 3.3 | 1/16 | 3.0140e-02 | - | 8.5561e-01 | - |
| | 1/32 | 5.0667e-03 | 1.09 | 1.4821e-01 | 1.06 |
| | 1/64 | 2.4832e-03 | 1.11 | 7.5659e-02 | 1.04 |
| | 1/128 | 1.2292e-03 | 1.12 | 3.7426e-02 | 1.05 |

We now compare the efficiency of the three schemes proposed in this work. The numerical solutions are carried out on the same hardware platform. The comparison results for the three methods are described in Tables 1–3 with the fine mesh $h = 1/256$. The accuracy of the velocity $\boldsymbol{u}$ with the $L^2$-norm are measured at the same fixed time, and the requisite CPU time for the three schemes is also listed.

It can be seen that Algorithm 3.1 (the common fully discrete finite element method) cannot achieve the error level $O(10^{-4})$ for the non-Newtonian cases $r = 1.5$ and $r = 1.8$. Moreover, the efficiency of Algorithm 3.3 (the artificial viscosity penalty projection FEM) can be seen, in addition to the reduced computing time compared with the other two methods for both Newtonian and non-Newtonian blood flows. In short, the artificial viscosity penalty finite element scheme has a relatively higher convergence order in space and demands less CPU time for solving the power-law Navier-Stokes equations.

**Table 2.** Numerical errors and convergence orders for the velocity field $\boldsymbol{u}$ and the pressure $p$ in spatial direction with $\tau = 10^{-3}$ and $r = 1.8$.

| Method | $h$ | $\|\boldsymbol{u}(t^n) - \boldsymbol{U}_h^n\|$ | Rate | $\|p(t^n) - P_h^n\|$ | Rate |
|---|---|---|---|---|---|
| Algorithm 3.1 | 1/16 | 8.1179e-02 | - | 9.2354e-01 | - |
| | 1/32 | 8.3604e-03 | 1.58 | 9.9241e-02 | 1.60 |
| | 1/64 | 4.1387e-03 | 1.59 | 4.7084e-02 | 1.59 |
| | 1/128 | 2.0487e-03 | 1.60 | 2.3308e-02 | 1.60 |
| Algorithm 3.2 | 1/16 | 4.6892e-02 | - | 8.7650e-01 | - |
| | 1/32 | 4.6399e-03 | 1.62 | 8.5866e-02 | 1.63 |
| | 1/64 | 2.2514e-03 | 1.65 | 4.3364e-02 | 1.62 |
| | 1/128 | 1.1484e-03 | 1.63 | 2.1682e-02 | 1.62 |
| Algorithm 3.3 | 1/16 | 2.9566e-02 | - | 8.4897e-01 | - |
| | 1/32 | 2.7551e-03 | 1.68 | 8.2341e-02 | 1.64 |
| | 1/64 | 1.3909e-03 | 1.67 | 4.2002e-02 | 1.62 |
| | 1/128 | 6.8194e-04 | 1.69 | 2.0792e-02 | 1.63 |

**Table 3.** Comparison of CPUtime for Algorithms 3.1–3.3 with different values of $r$.

| $r$ | Accuracy | Algorithm 3.1 | Algorithm 3.2 | Algorithm 3.3 |
|---|---|---|---|---|
| $r = 1.5$ | $O(10^{-1})$ | 29.87 s | 16.44 s | 8.16 s |
| | $O(10^{-2})$ | 213.20 s | 128.73 s | 83.31 s |
| | $O(10^{-3})$ | 684.36 s | 282.90 s | 195.42 s |
| | $O(10^{-4})$ | * * * | 495.35 s | 319.89 s |
| $r = 1.8$ | $O(10^{-1})$ | 25.66 s | 14.78 s | 7.47 s |
| | $O(10^{-2})$ | 196.87 s | 122.29 s | 79.95 s |
| | $O(10^{-3})$ | 674.12 s | 279.53 s | 187.80 s |
| | $O(10^{-4})$ | * * * | 484.21 s | 308.43 s |
| $r = 2.0$ | $O(10^{-1})$ | 16.85 s | 8.69 s | 4.08 s |
| | $O(10^{-2})$ | 120.49 s | 94.32 s | 50.16 s |
| | $O(10^{-3})$ | 548.53 s | 210.48 s | 140.28 s |
| | $O(10^{-4})$ | 873.68 s | 420.70 s | 284.75 s |

### 5.2. *Blood flow in aortic aneurysms*

In this set of numerical examples, we utilize a previously employed artificial viscosity penalty projection finite element code to perform a number of simulations for both non-Newtonian ($r = 1.8$) and Newtonian ($r = 2.0$) blood flow behavior in aortic aneurysms. Figures 1 and 2 show the geometric models and the computational grids for a fusiform aneurism and saccular aneurism, respectively. Figure 3 gives a comparison of the magnitude of velocity between the Newtonian and non-Newtonian behavior of blood flow in the case of a fusiform aneurism. The flow suggests that the Newtonian model predicts more complex flow structures downstream of the fusiform aneurysm than the non-Newtonian model. Moreover, the Newtonian model exhibits a recirculation vortex in the aneurysm region that is found significant compared with the non-Newtonian model. Moreover, the non-Newtonian model displays the lower values of velocity at Location A (shown in Figure 4) than the non-Newtonian case due to the shear-thinning characteristics of non-Newtonian blood viscosity. Similarly, in Figures 5 and 6, it is noticeable that the differences between the magnitude of Newtonian and non-Newtonian velocity become more observable in the saccular aneurism region. Our findings indicate that the turbulent velocity fields are significantly for Newtonian properties in pathologically altered configurations. In addition, the non-Newtonian fluid is found to have a lower velocity than the Newtonian fluid at Location B. From a flow mechanics standpoint, one can predict that the geometry of an aneurysm will alter the blood flow patterns and hemodynamic stresses within the aneurysm. Furthermore, substances such as proteins, lipoproteins, platelets, red blood cells, lymphocytes, monocytes, and neutrophils in human blood will be aggregated due to the lower velocity and the weaker recirculation vortex within aortic aneurysms. The assumption that the Newtonian blood viscosity model might be overestimating the fluid velocity at the risk of rupture in intracranial aneurysms. Therefore, these findings highlight the importance of considering the non-Newtonian properties of blood flow within aneurysms when studying the risk of aneurysm rupture.

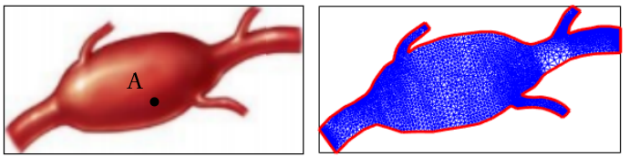


**Figure 1.** Geometry model of aortic aneurisms. (a) Fusiform aneurism; (b) computational grids in a two-dimensional (2D) profile model of a fusiform aneurism.

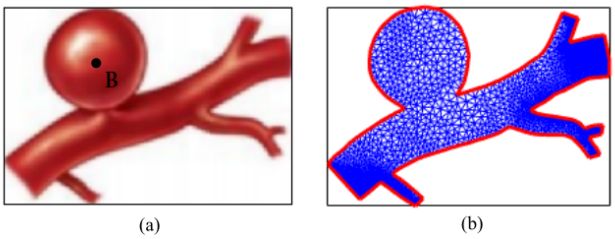


**Figure 2.** Geometry model of an aortic aneurism. (a) Saccular aneurism; (b) computational grids in a two-dimensional (2D) profile model of a saccular aneurism.

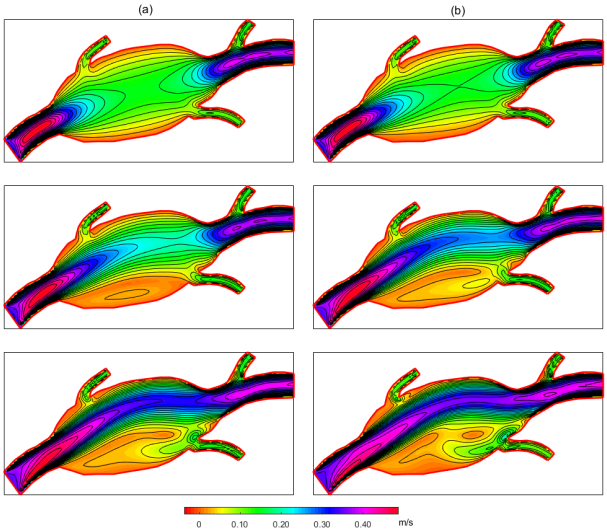


**Figure 3.** Comparison of the magnitude of velocity between the non-Newtonian (left column) and Newtonian (right column) behavior of blood flow in the case of fusiform aneurism at time $t = 0.1\text{s}, 0.4\text{s}$, and $0.8\text{s}$. The graphs are arranged column-wise.

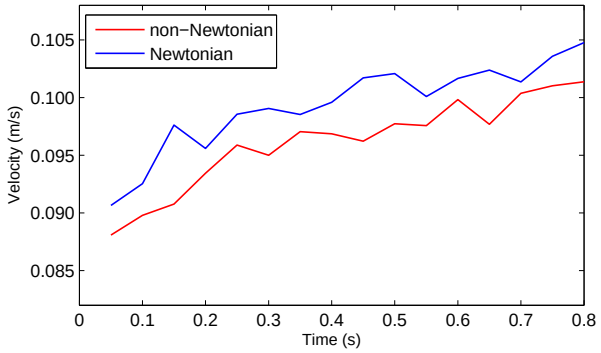


**Figure 4.** Comparison of the magnitude of velocity between the Newtonian and non-Newtonian behavior of blood flow at Location A shown in Figure 1(a).

### *5.3. Patient-specific cerebral aneurysms*

Clinical methods for diagnosing diseased cerebral arteries can only measure elementary blood velocity. At the same time, to understand the causes of these occurrences, it is necessary to obtain information about the amount of pressure possible through computational models. The endovascular treatment of diseased arteries demands the implementation of platinum coil embolization and flow diversion devices. There is a compelling demand to figure out the essential characteristics associated with the various normal and disturbed flow conditions in order to detect the afflicted areas in the coronary artery with variation in the accumulated plaque. Moreover, the doctors diagnosing the patient with a blockage in the artery should know the cardiovascular pathologies. For this, understanding blood's rheology is crucial, which can be performed by considering computational fluid dynamic models.

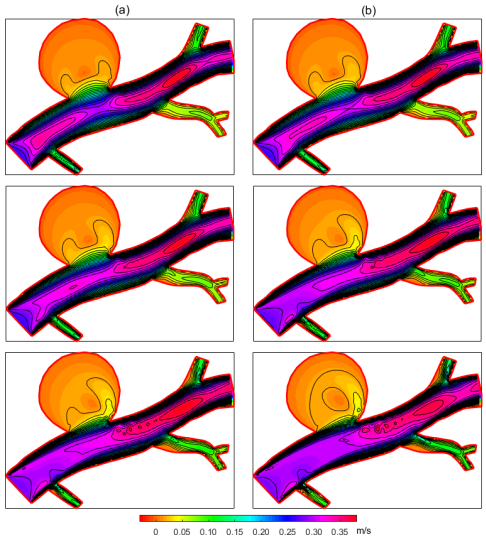


**Figure 5.** Comparison of the magnitude of velocity between the (a) non-Newtonian and (b) Newtonian behavior of blood flow in case of a saccular aneurism at time $t = 0.1$s, 0.4s, and 0.8s. The graphs are arranged column-wise.

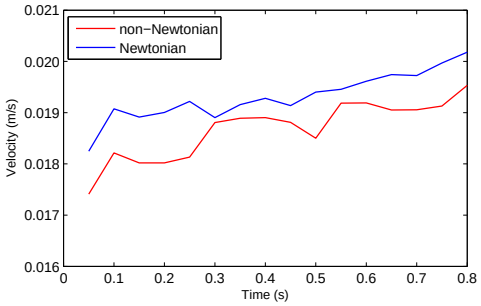


**Figure 6.** Comparison of the magnitude of velocity between the Newtonian and non-Newtonian behavior of blood flow at Location B shown in Figure 4(a).

In practice, patient-specific simulations of aneurysms can be constructed by using computational fluid dynamic techniques and images based vascular models through segmentation of magnetic resonance imaging (MRI) or computed tomography angiography (CTA). In this test, two patient-specific cerebral aneurysms from MRI and the corresponding computational domains are shown in Figures 7(a),(b) and 8(a),(b). Figures 7(c) and 8(c) exhibit the geometric models and the computational grids for a fusiform aneurism and saccular aneurism, respectively. We also use the artificial viscosity penalty projection finite element code to simulate the blood flows for patient-specific cerebral aneurysms. In the case of the non-Newtonian flow, the blood viscosity, density, and power-law index are assumed to be $\eta_0 = 0.012171\text{Pa} \cdot \text{s}$, $\rho = 1.06\text{g/cm}^3$, and $r = 1.7991$, respectively. These input parameters are based on theoretical studies and by fitting the parameters to experimental blood viscosity data obtained at certain shear rates (see [42, 43]). We are interested in plotting the magnitude of velocity and pressure distributions for the cases of fusiform and saccular aneurism, which are shown in Figures 9 and 10, respectively. We find that the region located near the center of the cross-sectional of cerebral blood vessels, which are characterized by high velocity, followed by the low values in the region of cerebral

aneurysms, as well as the weaker recirculation vortex, usually appears in these low-velocity regions within fusiform aneurisms or saccular aneurisms. The substance might be aggregated at a lower velocity within aneurism regions. It also can be seen that the pressure distributions at the curved part of the vessels change dramatically, but not distinctly in the regions of the fusiform aneurism or the saccular aneurism. This information can be of importance in the investigation of cerebrovascular diseases, and could be used as a hematological factor to assess the risk of rupture of the aneurysm. It should be pointed out that the simulation results have been provided to vascular surgeons for selecting the best surgical procedure for the patients.

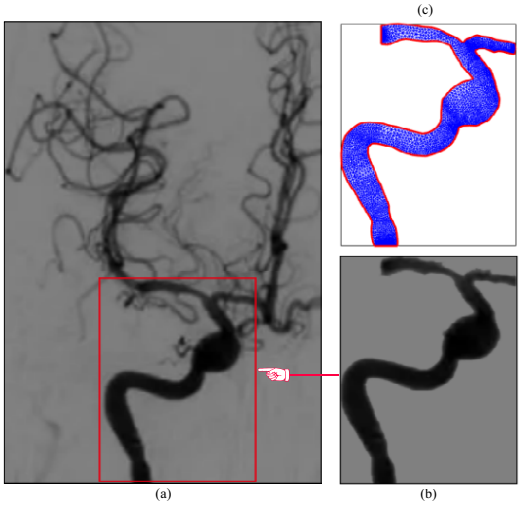


**Figure 7.** Basic model of a fusiform cerebral aneurysm. (a) Patient's medical imaging. (b) Computational domain associated with the red square inside Image (a). (c) Geometric structure and computational grids of a realistic aneurysm reconstructed from Image (b).

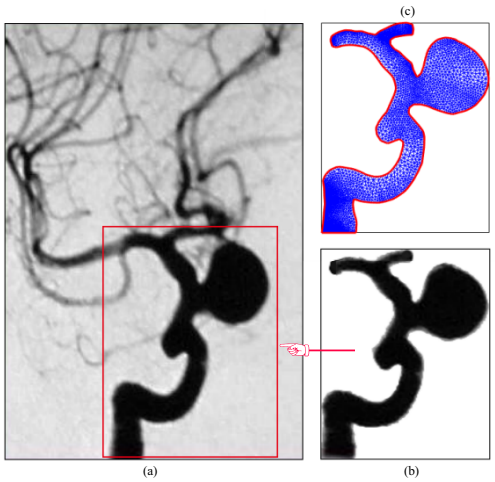


**Figure 8.** Basic model of a saccular cerebral aneurysm. (a) Patient's medical imaging. (b) Computational domain associated with the red square inside Image (a). (c) Geometric structure and computational grids of realistic aneurysm reconstructed from Image (b).

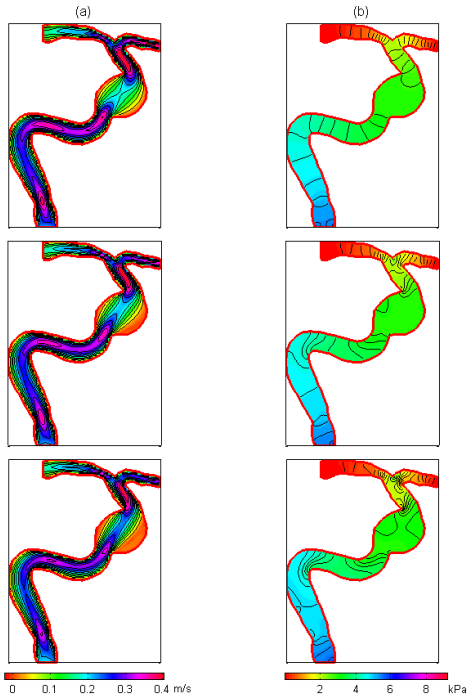


**Figure 9.** Snapshots of the (a) velocity and (b) pressure distributions for the case of a fusiform cerebral aneurysm.

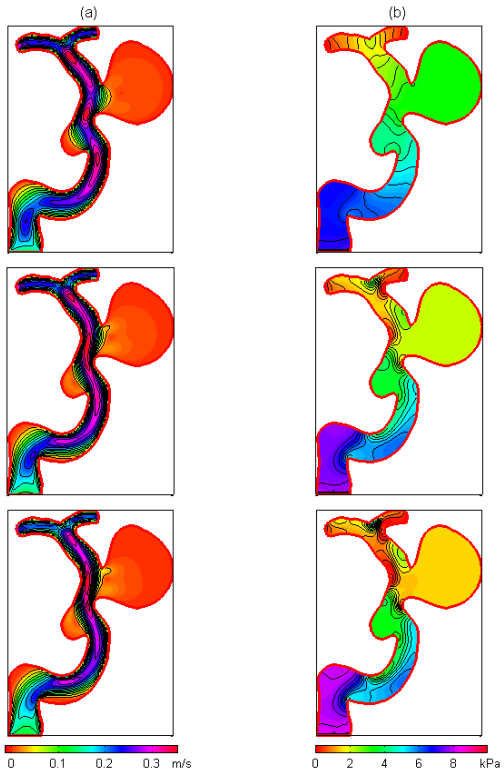


**Figure 10.** Snapshots of the (a) velocity and (b) pressure distributions for the cases of a saccular cerebral aneurysm.

## 6. Conclusion remarks

In this paper, we propose and develop new artificial viscosity penalty projection finite element methods for solving the power-law Navier-Stokes equations. The mathematical foundation and numerical analysis of the proposed schemes are also rigorously established. The numerical results also show of the proposed method can achieve the desired computational efficiency in the sense that a slightly higher convergence order and less CPU time. Another main goal of this work is to assess the difference between Newtonian and non-Newtonian viscosity models of blood flow in aortic aneurysms. This work suggests that the use of a non-Newtonian viscosity models may be attractive for solving blood flows, since it can provide simulation results that are presumably physically more realistic with at least comparable computational effort for a given level of accuracy. In addition, two patient-specific simulations of cerebral aneurysms have been performed, which could help vascular surgeons in diagnosing the diseased cerebral arteries, assessing the risk of rupture of the aneurysm, and selecting the best surgical procedure for the patients. Other aspects of our ongoing work, including a study of the predictive value of risk factors for aneurysm rupture in viscoelastic vessels, aim to evaluate the clinical value of intervention in the diagnosis and treatment of aneurysms.

## Acknowledgements

G. Zou is partially supported by the Key Scientific Research Projects of Colleges and Universities in Henan Province, China (23A110006); the Foundation for University Youth Key Teacher of Henan Province of China (2023GGJS017); and the Natural Science Foundation of Henan Province (252300420310).

## References

1. K. B. Chandran, S. E. Rittgers, A. P. Yoganathan, *Biofluid Mechanics: The Human Circulation*, $2^{nd}$ Edition, CRC Press, 2012. https://doi.org/10.1201/b11709
2. K. Chitra, S. Vengadesan, T. Sundararajan, P. Nithiarasu, An investigation of pulsatile flow in a model cavo-pulmonar vascular system, *Commun. Numer. Methods Eng.*, **25** (2009), 1061–1083. https://doi.org/10.1002/cnm.1205
3. S. N. Majhi, V. R. Nair, Pulsatile flow of third grade fluids under body acceleration-modelling blood flow, *Int. J. Eng. Sci.*, **32** (1994), 839–846. https://doi.org/10.1016/0020-7225(94)90064-7
4. J. G. Myers, J. A. Moore, M. Ojha, K. W. Johnston, C. R. Ethier, Factors influencing blood row patterns in the human right coronary artery, *Ann. Biomed. Eng.*, **29** (2001), 109–120. https://doi.org/10.1114/1.1349703
5. T. W. H. Sheu, S. F. Tsai, W. S. Hwang, T. M. Chang, A finite element study of the blood flow in total cavopulmonary connection, *Comput. Fluids*, **28** (1999), 19–39. https://doi.org/10.1016/S0045-7930(98)00018-8
6. R. Budwig, D. Eiger, H. Hooper, J. Slippy, Steady flow in abdominal aortic aneurysm models, *ASME J. Biomech. Eng.*, **115** (1993), 418–423. https://doi.org/10.1115/1.2895506

7. J. R. Cebral, M. A. Castro, J. E. Burgess, R. S. Pergolizzi, M. J. Sheridan, C. M. Putman, Characterization of cerebral aneurysms for assessing risk of rupture by using patient-specific computational hemodynamics models, *Am. J. Neuroradiol.*, **26** (2005), 2550–2559.
8. M. Julia, J. G. Bernard, Pulsatile flow in model cerebral aneurysms, *Procedia Comput. Sci.*, **4** (2011), 811–820. https://doi.org/10.1016/j.procs.2011.04.086
9. Z. Li, C. Kleinstreurer, Blood flow and structure interaction in a stented abdominal aortic aneurysm model, *Med. Eng. Phys.*, **27** (2005), 369–382. https://doi.org/10.1016/j.medengphy.2004.12.003
10. S. A. Berger, L. D. Jou, Flows in stenotic vessels, *Annu. Rev. Fluid Mech.*, **32** (2000), 347–382. https://doi.org/10.1146/annurev.fluid.32.1.347
11. A. D. Caballero, S. Laín, Numerical simulation of non-Newtonian blood flow dynamics in human thoracic aorta, *Comput. Methods Biomech. Biomed. Eng.*, **18** (2015), 1200–1216. https://doi.org/10.1115/1.2895506
12. F. J. H. Gijsen, F. N. V. de Vosse, J. D. Janssen, The influence of the non-Newtonian properties of blood on the flow in large arteries: Steady flow in a carotid bifurcation model, *J. Biomech.*, **32** (1999), 601–608. https://doi.org/10.1016/s0021-9290(99)00015-9
13. E. Gudiño, C. M. Oishi, A. Sequeira, Influence of non-Newtonian blood flow models on drug deposition in the arterial wall, *J. Non-Newtonian Fluid Mech.*, **274** (2019), 104206. https://doi.org/10.1016/j.jnnfm.2019.104206
14. B. M. Johnston, P. R. Johnston, S. Comey, D. Kilpatrick, Non-Newtonian blood flow in human right coronary arteries: Steady state simulations, *J. Biomech.*, **37** (2004), 709–720. https://doi.org/10.1016/j.jbiomech.2003.09.016
15. X. Liu, Y. Fan, X. Deng, F. Zhan, Effect of non-Newtonian and pulsatile blood flow on mass transport in the human aorta, *J. Biomech.*, **44** (2011), 1123–1131. https://doi.org/10.1016/j.jbiomech.2011.01.024
16. V. L. Marrero, J. A. Tichy, O. Sahni, K. E. Jansen, Numerical study of purely viscous non-Newtonian flow in an abdominal aortic aneurysm, *J. Biomech. Eng.*, **136** (2014), 101001. https://doi.org/10.1115/1.4027488
17. J. Bernsdorf, D. Wang, Non-Newtonian blood flow simulation in cerebral aneurysms, *Comput. Math. Appl.*, **58** (2009), 1024–1029. https://doi.org/10.1016/j.camwa.2009.02.019
18. J. Deteix, D. Yakoubi, Shear rate projection schemes for non-Newtonian fluids, *Comput. Method. Appl. Mech. Eng.*, **354** (2019), 620–636. https://doi.org/10.1016/j.cma.2019.06.006
19. H. G. Morales, I. Larrabide, A. J. Geers, M. L. Aguilar, A. F. Frangi, Newtonian and non-Newtonian blood flow in coiled cerebral aneurysms, *J. Biomech.*, **46** (2013), 2158–2164. https://doi.org/10.1016/j.jbiomech.2013.06.034
20. K. Perktold, R. Peter, M. Resch, Pulsatile non-Newtonian blood flow simulation through a bifurcation with an aneurysm, *Biorheology*, **26** (1989), 1011–1030. https://doi.org/10.3233/bir-1989-26605
21. V. L. Rayz, A. Abla, L. Boussel, J. R. Leach, G. Acevedo-Bolton, D. Saloner, et al., Computational modeling of flow-altering surgeries in basilar aneurysms, *Ann. Biomed. Eng.*, **43** (2014), 1210—1222. https://doi.org/10.1007/s10439-014-1170-x

22. S. Katz, A. Caiazzo, B. Moreau, Impact of turbulence modeling on the simulation of blood flow in aortic coarctation, *Int. J. Numer. Method Biomed. Eng.*, **39** (2023), e3695. https://doi.org/10.1002/cnm.3695

23. X. Zhang, B. Mao, Y. Che, J. Kang, M. Luo, Physics-informed neural networks (PINNs) for 4D hemodynamics prediction: An investigation of optimal framework based on vascular morphology, *Comput. Biol. Med.*, **164** (2023), 107287. https://doi.org/10.1016/j.compbiomed.2023.107287

24. F. He, L. Hua, T. Guo, Numerical modeling in arterial hemodynamics incorporating fluid-structure interaction and microcirculation, *Theor. Biol. Med. Model.*, **18** (2021), 6. https://doi.org/10.1186/s12976-021-00136-z

25. J. W. Barrett, W. B. Liu, Finite element error analysis of a quasi-Newtonian flow obeying the Carreauor power law, *Numer. Math.*, **64** (1993), 433–453. https://doi.org/10.1007/BF01388698

26. J. B. Barrett, W. B. Liu, Quasi-norm error bounds for the finite element approximation of a non-Newtonian flow, *Numer. Math.*, **68** (1994), 437–456. https://doi.org/10.1007/s002110050071

27. J. Baranger, P. Georget, K. Najib, Error estimates for a mixed finite element method for a non-Newtonian flow, *J. Non-Newtonian Fluid Mech.*, **23** (1987), 415–421. https://doi.org/10.1016/0377-0257(87)80029-0

28. L. Lefton, D. Wei, Penalty finite element approximations of the stationary power-law Stokes problem, *J. Numer. Math.*, **11** (2003), 301–322. https://doi.org/10.1515/156939503322663467

29. J. Borggaard, T. Iliescu, J. P. Roop, An improved penalty method for power-law Stokes problem, *J. Comput. Appl. Math.*, **223** (2009), 646–658. https://doi.org/10.1016/j.cam.2008.02.002

30. J. K. Djoko, J. M. Lubuma, M. Mbehou, On the numerical solution of the stationary power-law Stokes equations: A penalty finite element approach, *J. Sci. Comput.*, **69** (2016), 1058–1082. https://doi.org/10.1007/s10915-016-0227-4

31. J. N. Reddy, V. A. Padhye, A penalty finite element model for axisymmetric flows of non-Newtonian fluids, *Numer. Methods Partial Differ. Equations*, **4** (1988), 33–56.

32. J. L. Lions, Quelques méthodes de résolution des problèmes aux limites non linéaires, *Dunod*, 1969.

33. Y. N. He, Optimal error estimate of the penalty finite element method for the time-dependent Navier-Stokes equations, *Math. Comp.*, **74** (2005), 1201–1216. https://doi.org/10.1090/S0025-5718-05-01751-5

34. Y. N. He, J. Li, A penalty finite element method based on the Euler implicit/explicit scheme for the time-dependent Navier-Stokes equations, *J. Comput. Appl. Math.*, **235** (2010), 708–725. https://doi.org/10.1016/j.cam.2010.06.025

35. M. Jobelin, C. Lapuerta, J. C. Latché, P. Angot, B. Piar, A finite element penalty-projection method for incompressible fows, *J. Comput. Phys.*, **217** (2006), 502–518. https://doi.org/10.1016/j.jcp.2006.01.019

36. J. Shen, On error estimates of the penalty method for unsteady Navier-Stokes equations, *SIAM J. Numer. Anal.*, **32** (1995), 386–403. https://doi.org/10.1137/0732016

37. J. Shen, On error estimates of the projection methods for the Navier-Stokes equations: Second-order schemes, *Math. Comput.*, **65** (1996), 1039–1065. https://doi.org/10.1090/S0025-5718-96-00750-8

38. X. Wang, G. A. Zou, B. Wang, The stabilized penalty-projection finite element method for the Navier-Stokes-Cahn-Hilliard-Oono system, *Appl. Numer. Math.*, **165** (2021), 376–413. https://doi.org/10.1016/j.apnum.2021.03.004

39. Y. N. He, Two-level method based on finite element and Crank-Nicolson extrapolation for the time-dependent Navier-Stokes equations, *SIAM J. Numer. Anal.*, **41** (2003), 1263–1285. https://doi.org/10.1137/S0036142901385659

40. G. P. Galdi, *An Introduction to the Mathematical Theory of the Navier-Stokes Equations, Steady-State Problems*, Springer, New York, 2011. https://doi.org/10.1007/978-0-387-09620-9

41. V. Thomée, *Galerkin Finite Element Methods for Parabolic Problems*, Springer, 1984. https://doi.org/10.1137/1028090

42. Y. I. Cho, K. R. Kensey, Effects of the non-Newtonian viscosity of blood on flows in a diseased arterial vessel. Part 1: Steady flows, *Biorheology*, **28** (1991), 241–262. https://doi.org/10.3233/bir-1991-283-415

43. J. B. Zhang, Z. B. Kuang, Study on blood constitutive parameters in different blood constitutive equations, *J. Biomech.*, **33** (2000), 355–360. https://doi.org/10.1016/S0021-9290(99)00101-3


AIMS Press